Supplementary Material

Content

1. Purity Data of the Fragments

HPLC Method

Purity was confirmed by high-performance liquid chromatography (HPLC) on an Ultimate 3000 HPLC-System with UV Detection (Thermo Fisher Scientific, Dreieich, Germany). The system was equipped with a ReproSil-XR 120 C18, 5 µm, 150 mm x 4.6 mm column (Dr. Maisch GmbH, Ammerbuch-Entringen, Germany) with column temperature set to 25 °C. Mobile phase A was 10 mM phosphate buffer pH 2.3 and mobile phase B was MeOH. The flow rate was set to 0.5 mL per min with the following gradient: 0–9 min: 10-85% B, 9–13 min: 85% B, 13–14 min: 85-10% B, 14–18 min: 10% B. For analysis, the fragments were dissolved in ACN. For CA001 and VS002, an ACN/MeOH mixture in a ratio of 1+1 was required to achieve sufficient solubility. 5 µL of the compound solution was injected on the column. The purity of the compounds was then calculated as the relative AUC of the main peak of the chromatogram at 218, 254, or 280 nm depending on the absorbance properties of the individual fragment. Retention times, calculated purities and detection waves used for the evaluation are summarized in **Table S1.1**.

HPLC traces and NMR spectra

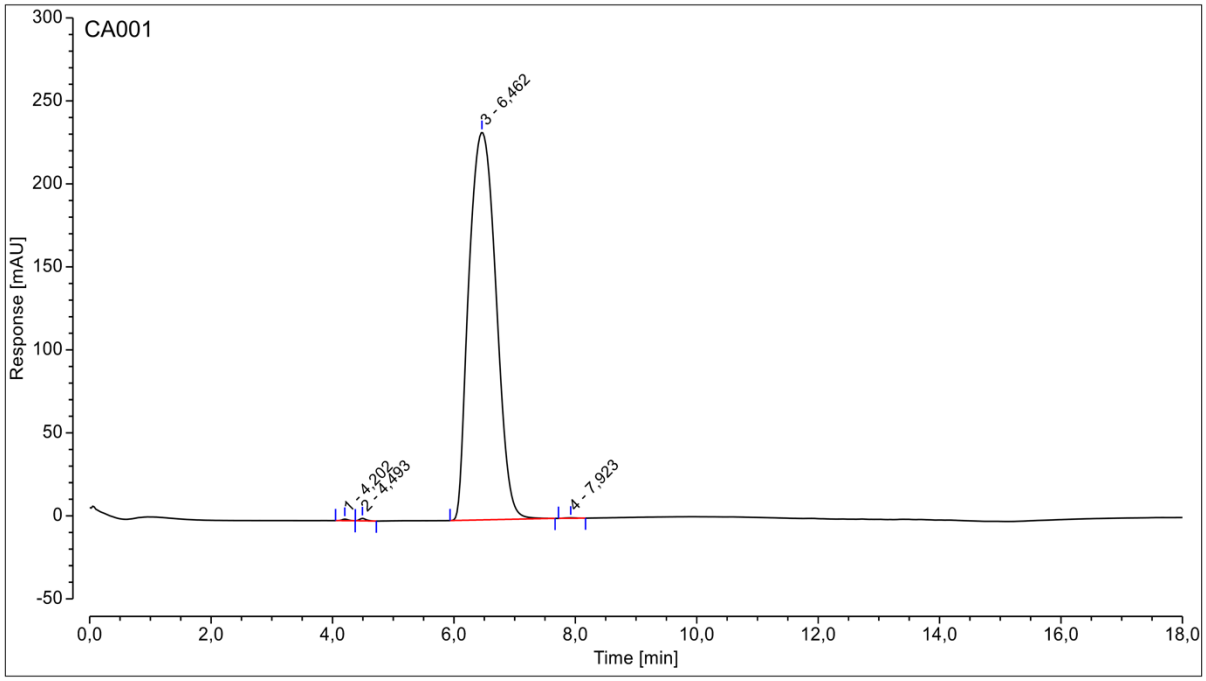

Figure S1.1: HPLC chromatogram of CA001. A retention time of 6.462 min with a relative purity of 99.72 % was determined for the compound at 254 nm detection wavelength.

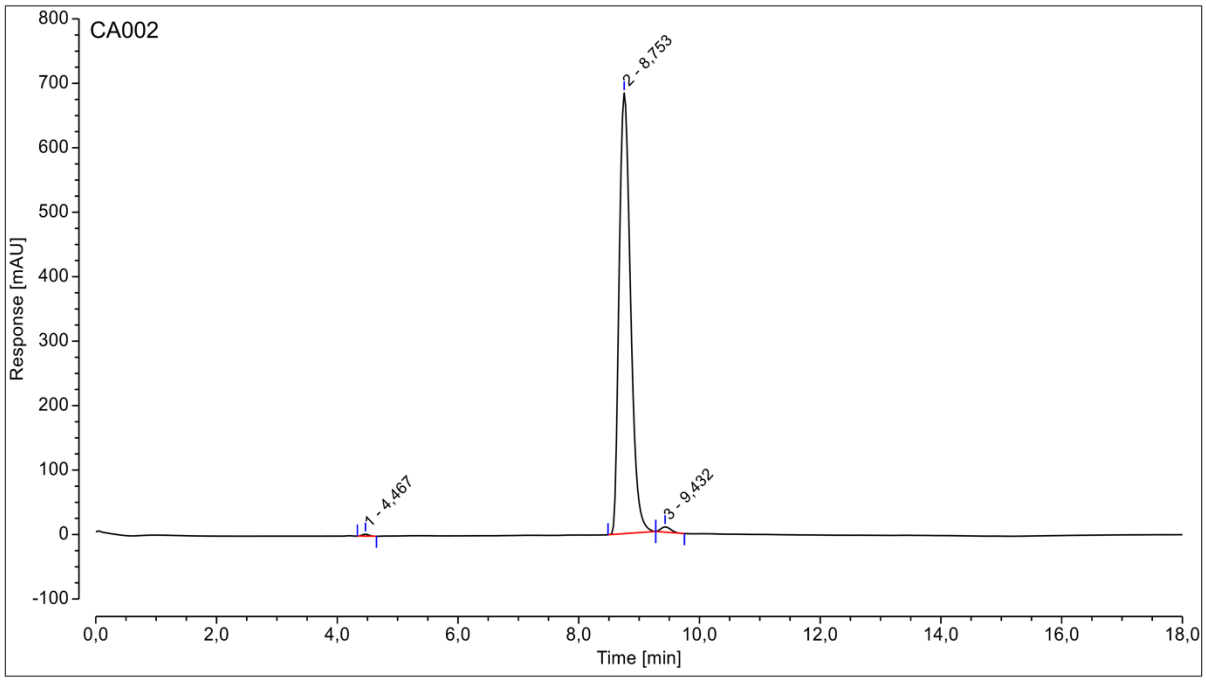

Figure S1.2: HPLC chromatogram of CA002. A retention time of 8.753 min with a relative purity of 98.75 % was determined for the compound at 254 nm detection wavelength.

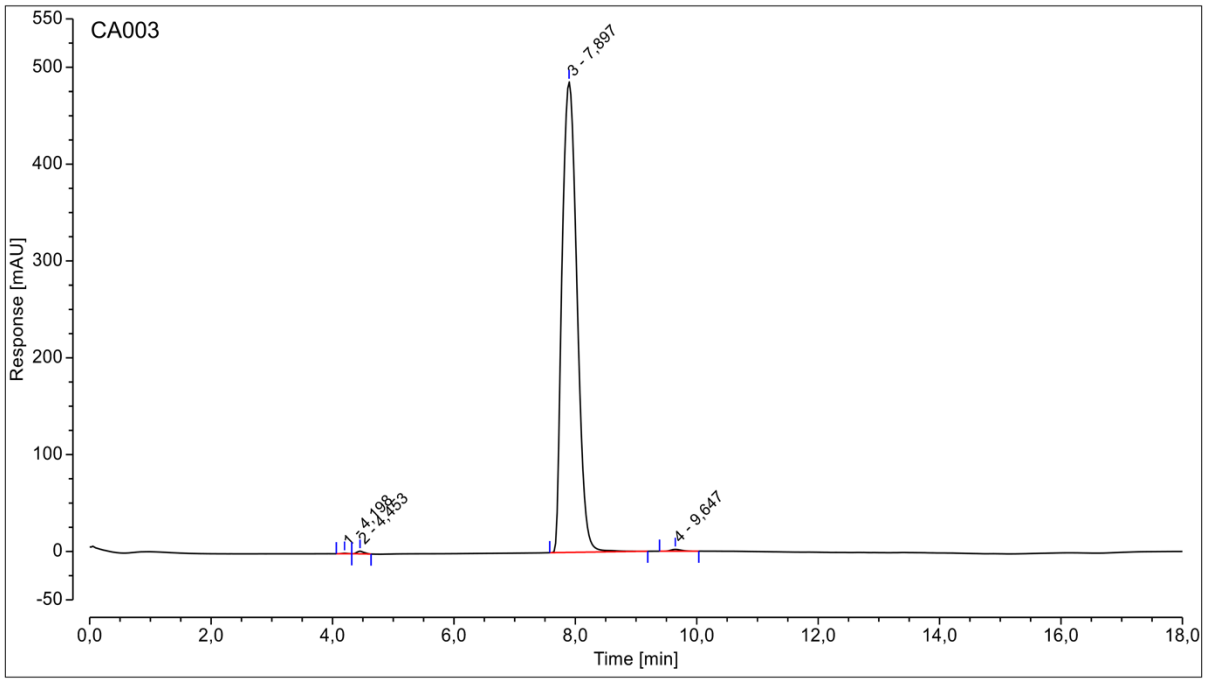

Figure S1.3: HPLC chromatogram of CA003. A retention time of 7.897 min with a relative purity of 99.44 % was determined for the compound at 254 nm detection wavelength.

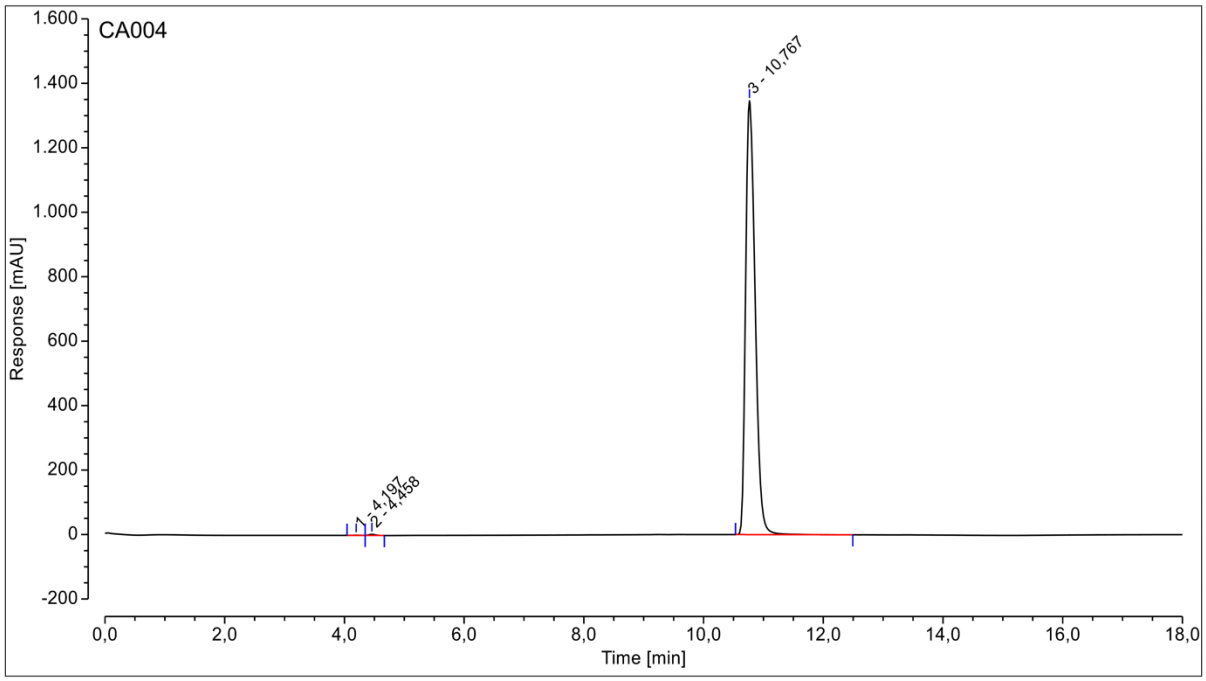

Figure S1.4: HPLC chromatogram of CA004. A retention time of 10.767 min with a relative purity of 99.81 % was determined for the compound at 254 nm detection wavelength.

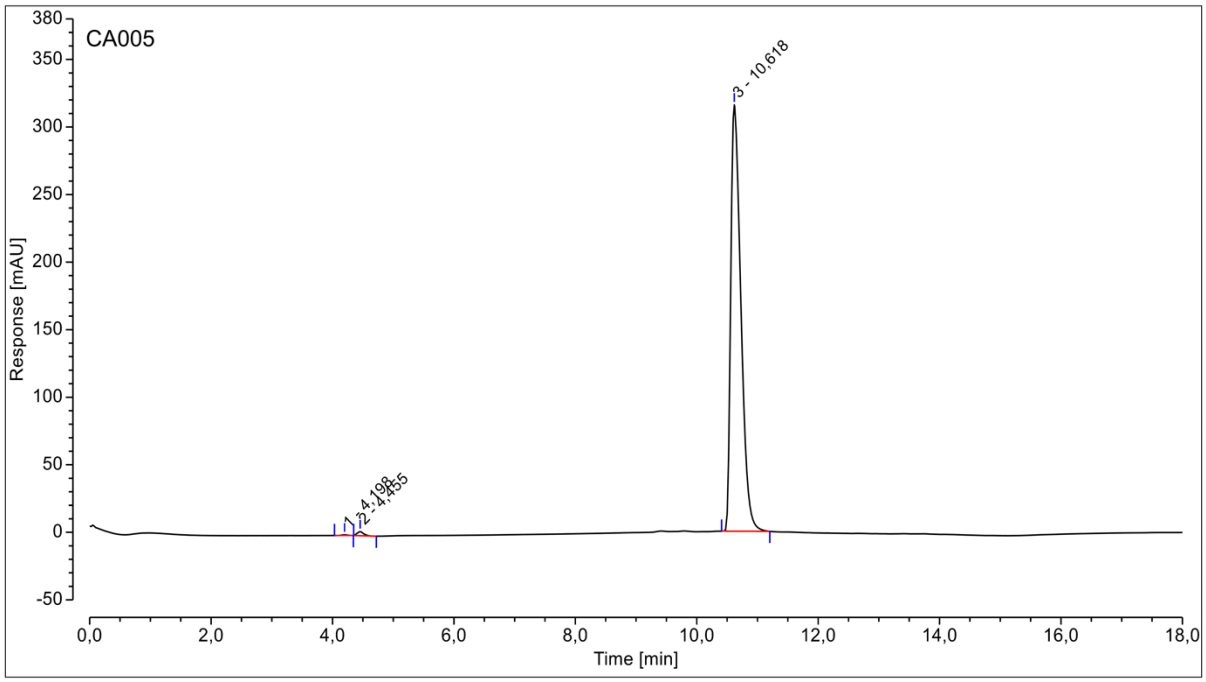

Figure S1.5: HPLC chromatogram of CA005. A retention time of 10.618 min with a relative purity of 99.29 % was determined for the compound at 254 nm detection wavelength.

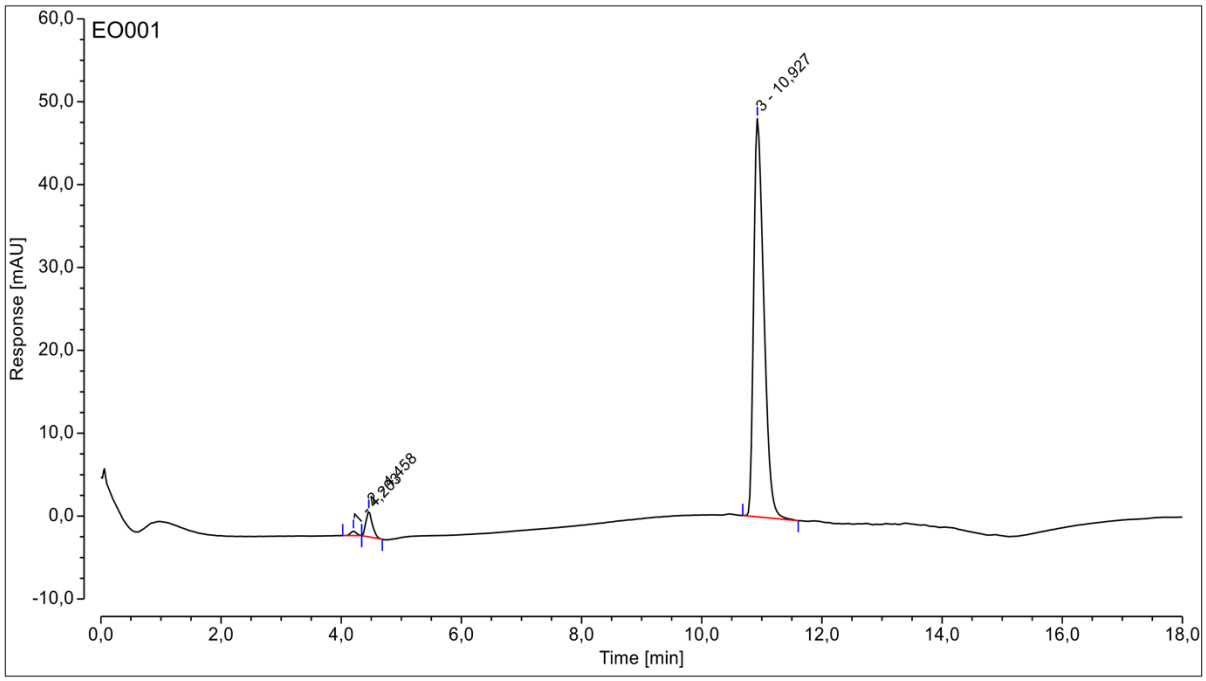

Figure S1.6: HPLC chromatogram of EO001. A retention time of 10.927 min with a relative purity of 92.99 % was determined for the compound at 254 nm detection wavelength.

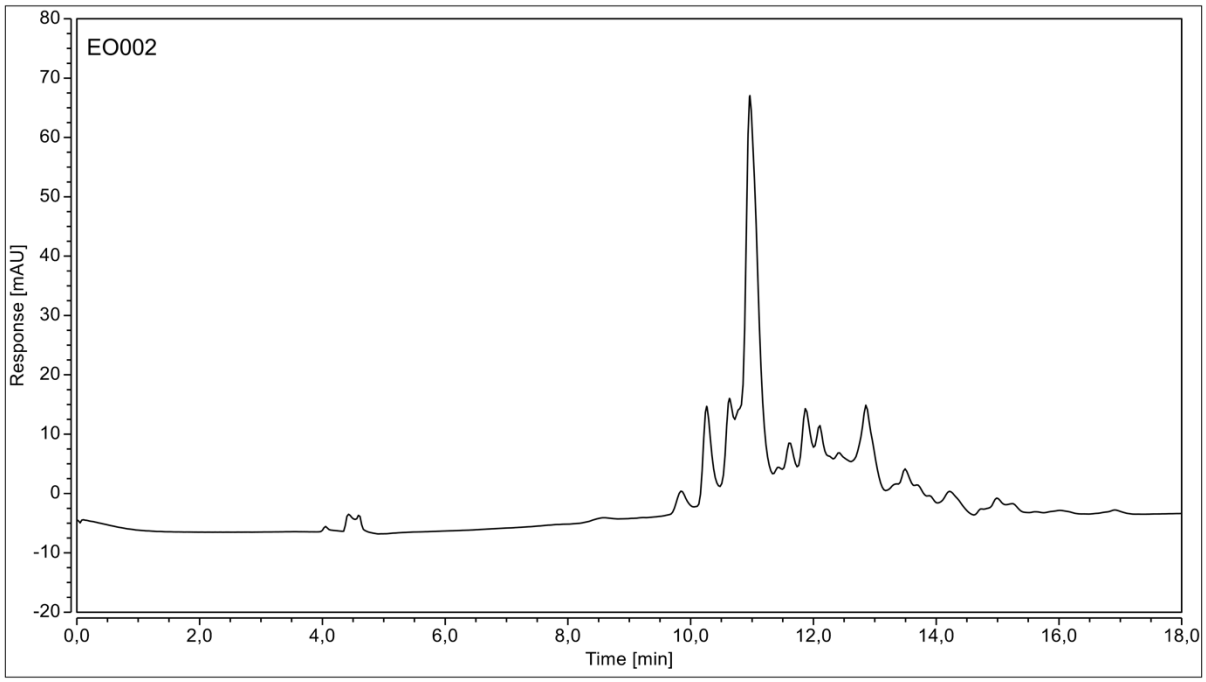

Figure S1.7: HPLC chromatogram of EO002. The chromatogram shows several unseparated peaks, which indicate a mixture of several components that were present in small amounts in the stock of the compound. Therefore, no distinct retention time and purity could be determined.

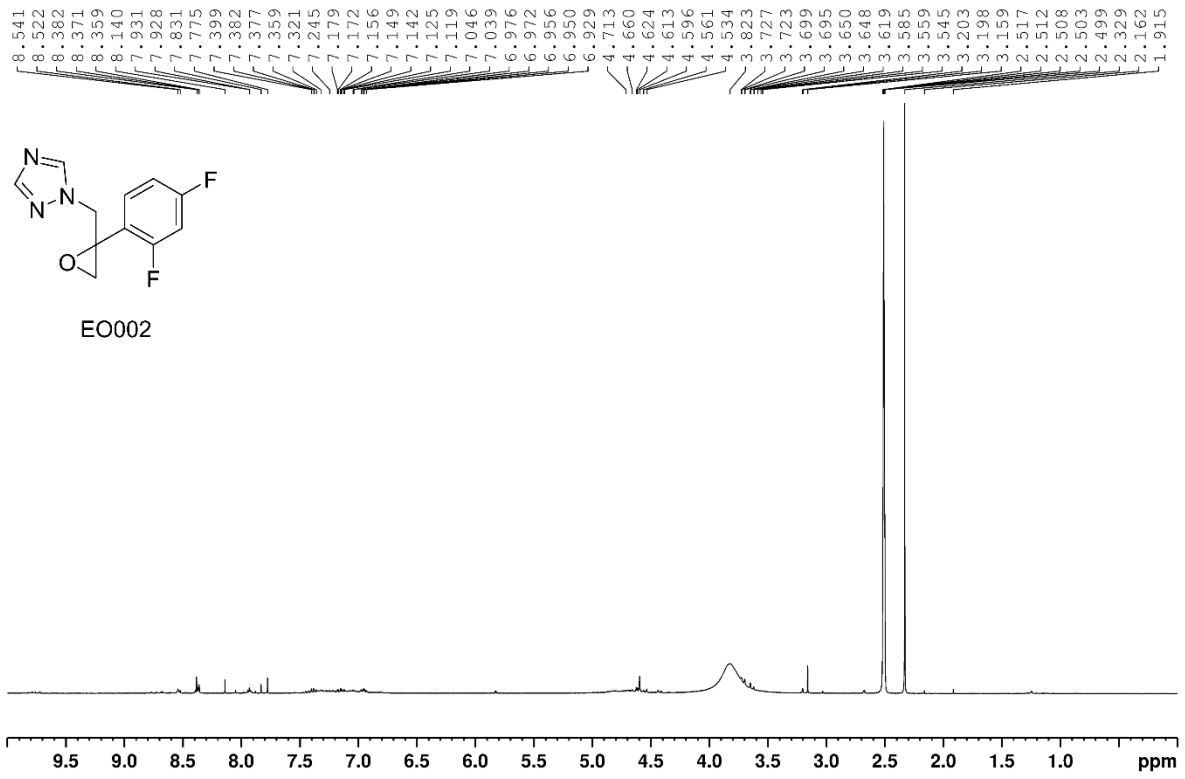

Figure S1.8: ^{1}H-NMR spectrum of EO002 DMSO-d_6. The spectrum shows one distinct singlet at 2.36 ppm. Additionally, several small peaks are visible whose integrals and shifts could not be associated to the aforementioned peak or the compound. The multiplet at 2.50 ppm could be assigned to the DMSO residual signal. In general, the spectrum could not be assigned to the given compound or its degradation products.

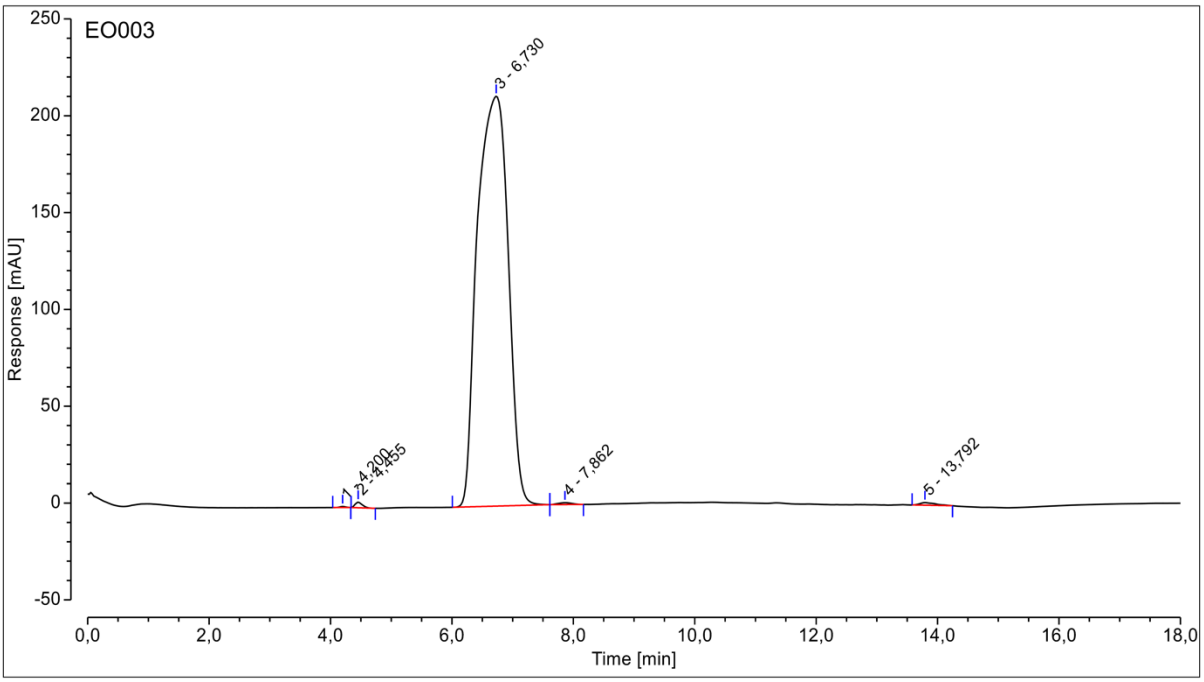

Figure S1.9: HPLC chromatogram of EO003. A retention time of 6.730 min with a relative purity of 99.12 % was determined for the compound at 254 nm detection wavelength.

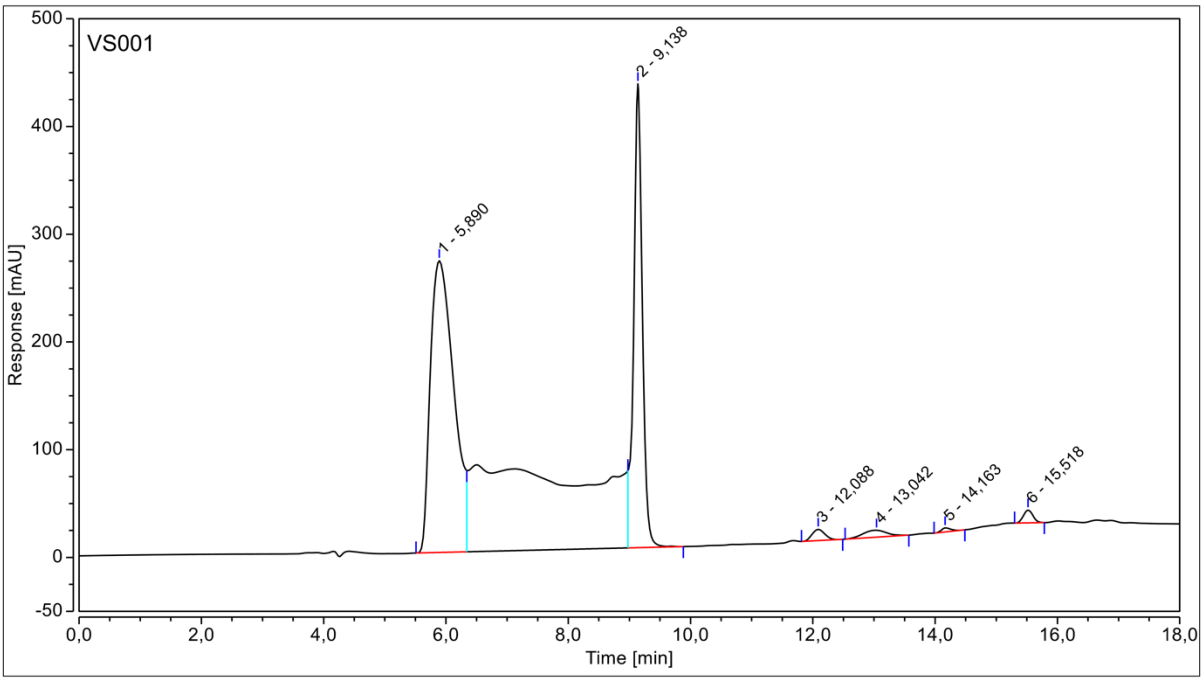

Figure S1.10: HPLC chromatogram of VS001. The chromatogram shows two peaks between 5 min and 9 min which blurred together. Therefore, no distinct retention time and purity could be determined. Further analysis was performed by ^{1}H-NMR (Figure S1.11).

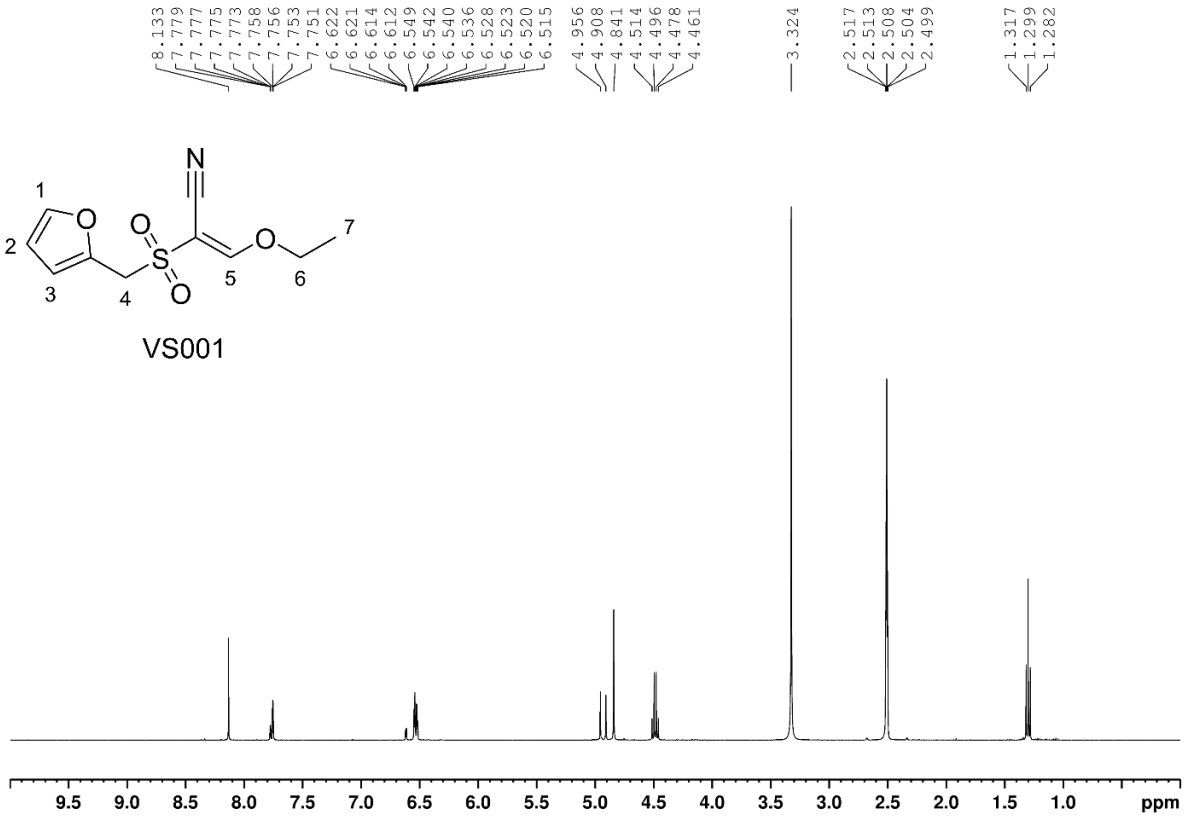

Figure S 11.11: ^{1}H-NMR spectrum of VS001 in DMSO-d_6. The following peaks could be assigned to the compound: δ = 1.29 (t, J =7.10 Hz, 3 H, 7), 2.50 (m, DMSO residual), 3.32 (s, water residual), 4.48 (q, J =7.10, 2 H, 6), 4.83 (s, 2 H, 4), 6.52 (m, 2 H, 2, 3), 7.76 (m, 1 H, 1), 8.13 s, 1H, 5). The Peaks: δ = 4.91 (s, 0.7 H), 4.96 (s, 0.6 H), 6.61 (m, 0.3 H) could not be assigned to the given compound. These peaks could be caused by potential unknown reversible or irreversible adduct formation. Nevertheless, the spectrum reveals that, compared to EO002, the major content is the indicated vinyl sulfone VS001.

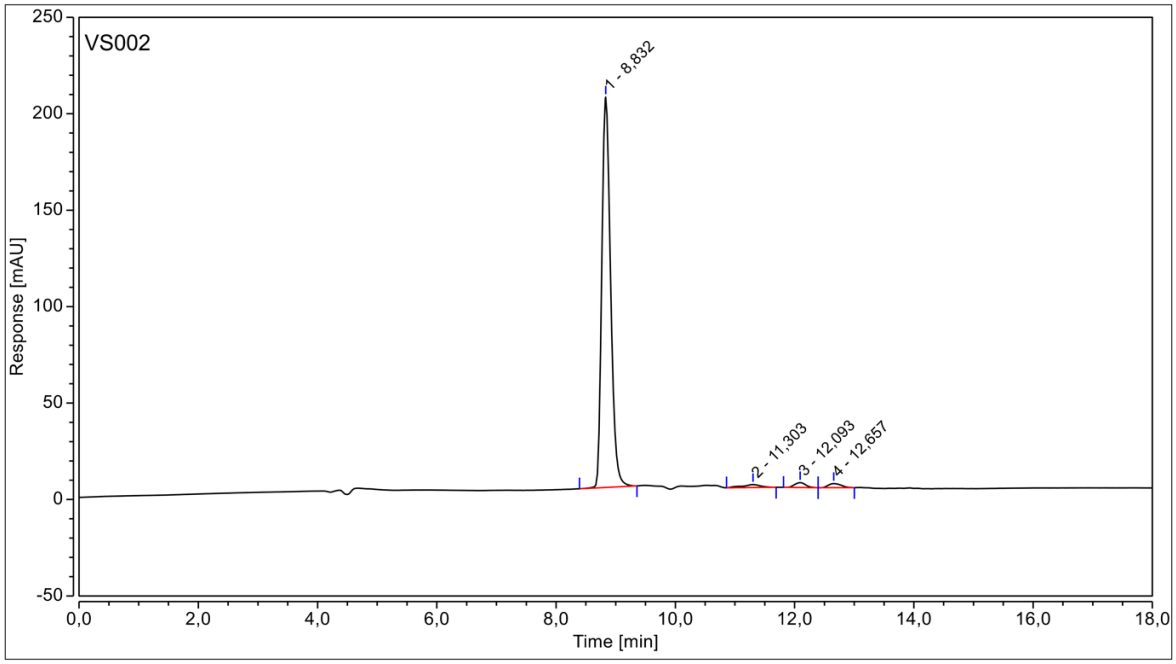

Figure S1.12: HPLC chromatogram of VS002. A retention time of 8.832 min with a relative purity of 95.50 % was determined for the compound at 280 nm detection wavelength.

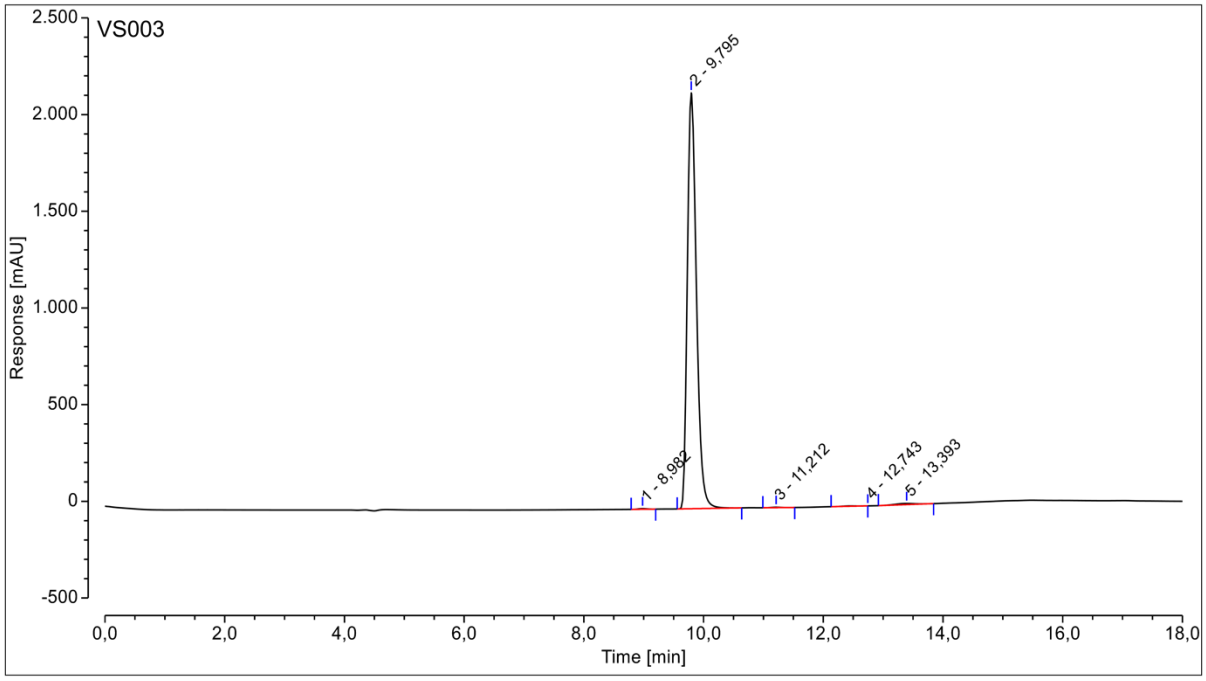

Figure S1.13: HPLC chromatogram of VS003. A retention time of 9.795 min with a relative purity of 99.04 % was determined for the compound at 218 nm detection wavelength.

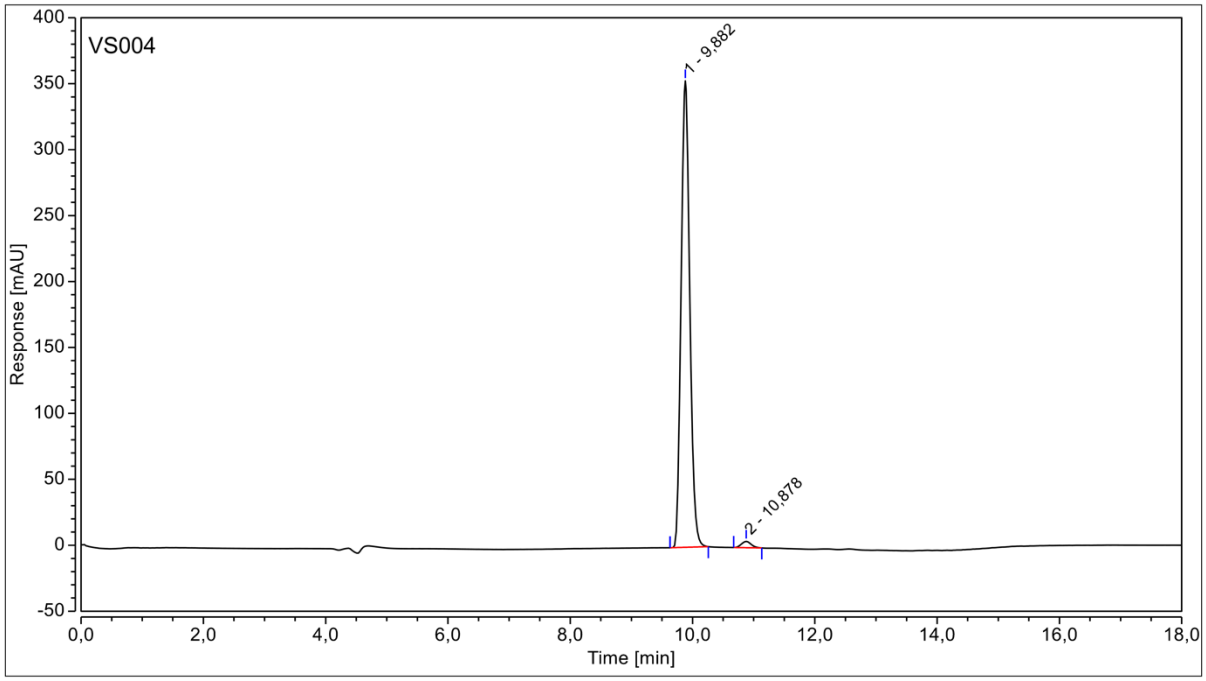

Figure S1.14: HPLC chromatogram of VS004. A retention time of 9.882 min with a relative purity of 98.67 % was determined for the compound at 254 nm detection wavelength.

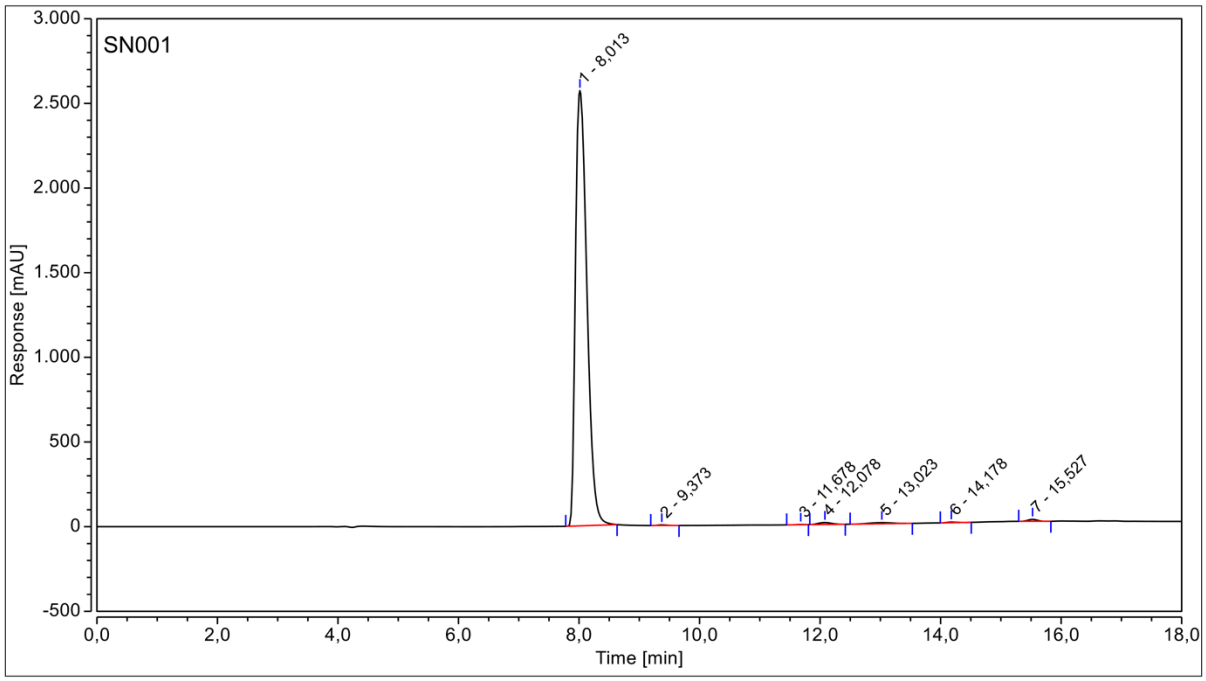

Figure S1.15: HPLC chromatogram of SN001. A retention time of 8.013 min with a relative purity of 98.36 % was determined for the compound at 218 nm detection wavelength.

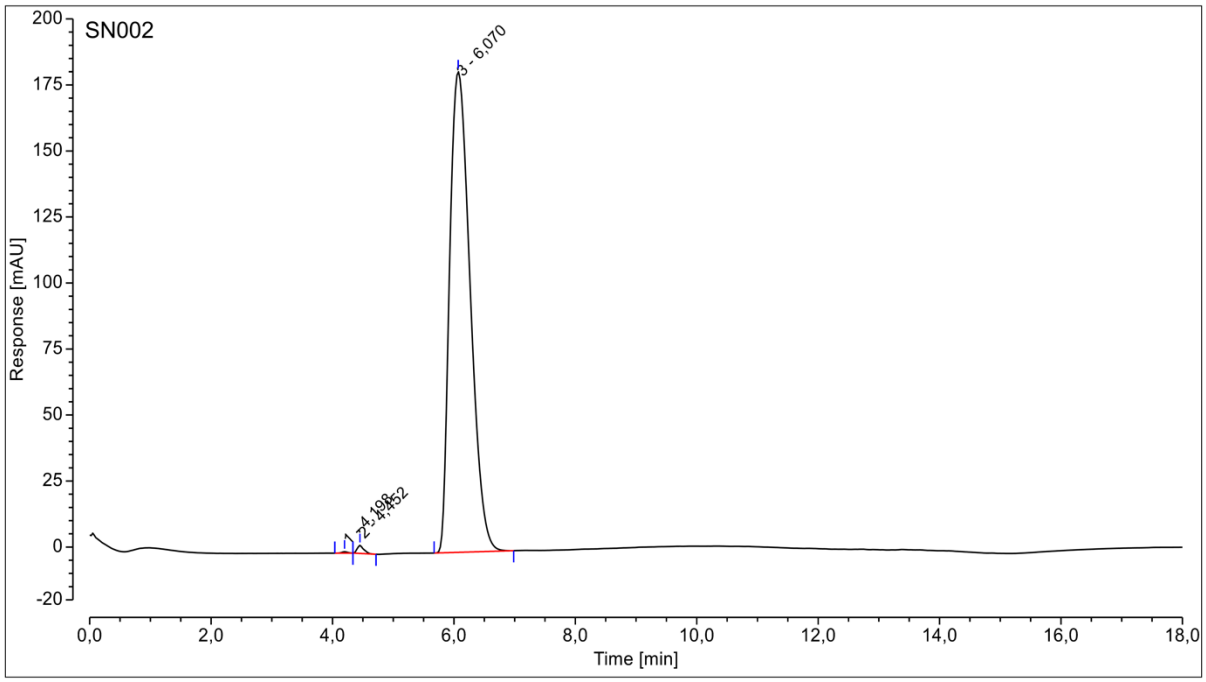

Figure S1.16: HPLC chromatogram of SN002. A retention time of 6.070 min with a relative purity of 99.38 % was determined for the compound at 254 nm detection wavelength.

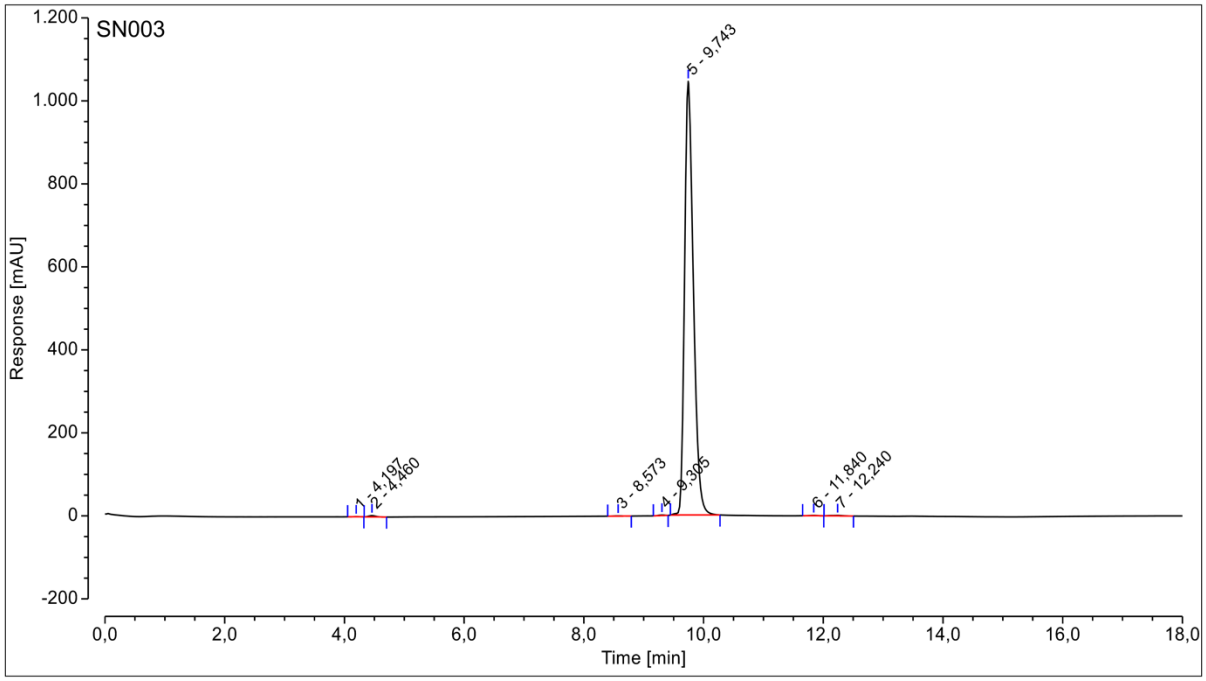

Figure S1.17: HPLC chromatogram of SN003. A retention time of 9.743 min with a relative purity of 99.36 % was determined for the compound at 254 nm detection wavelength.

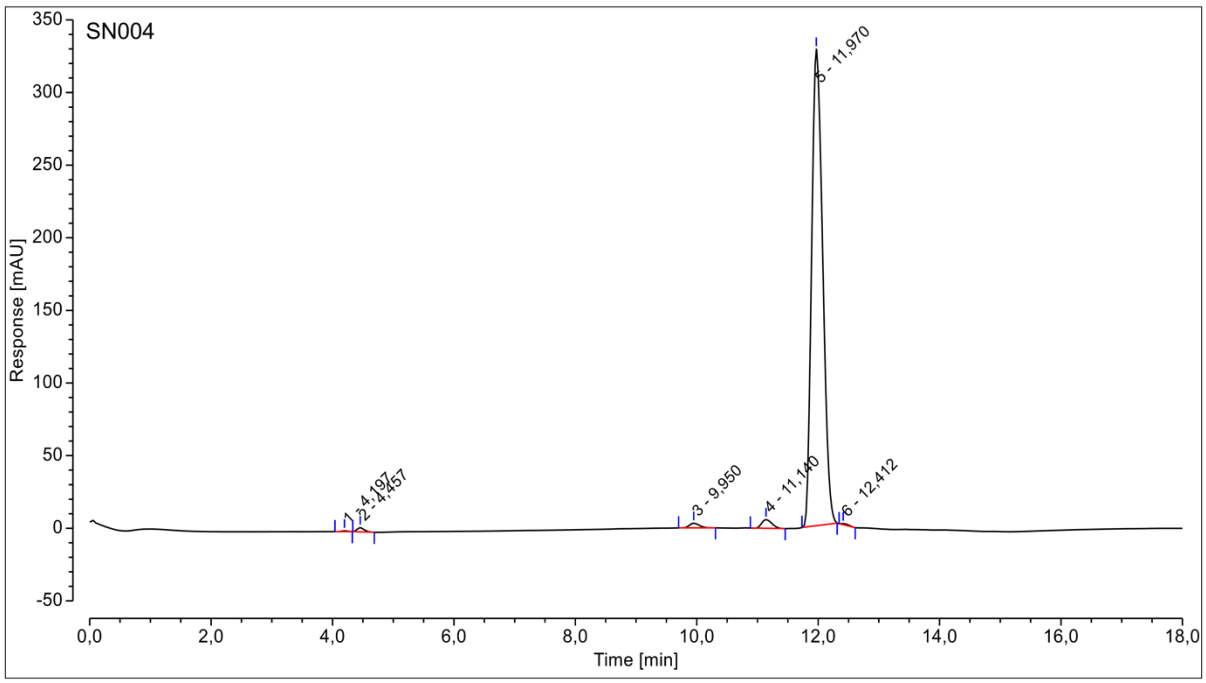

Figure S1.18: HPLC chromatogram of SN004. A retention time of 11.970 min with a relative purity of 96.73 % was determined for the compound at 254 nm detection wavelength.

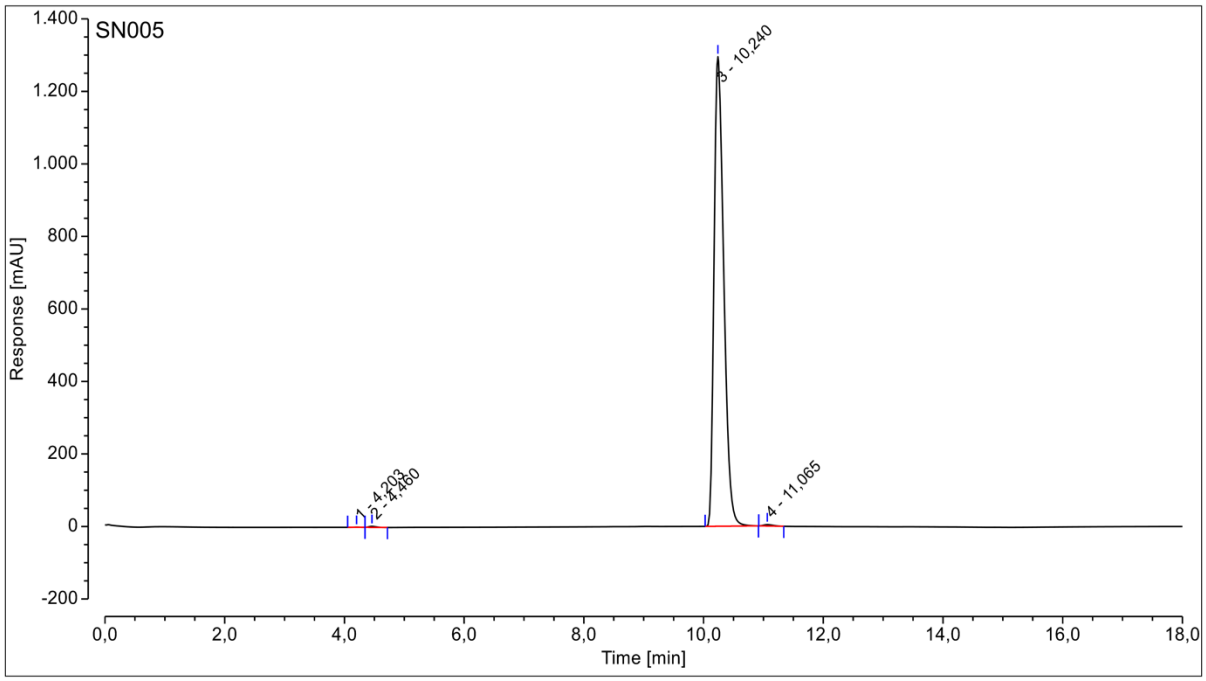

Figure S1.19: HPLC chromatogram of SN005. A retention time of 10.240 min with a relative purity of 99.54 % was determined for the compound at 254 nm detection wavelength.

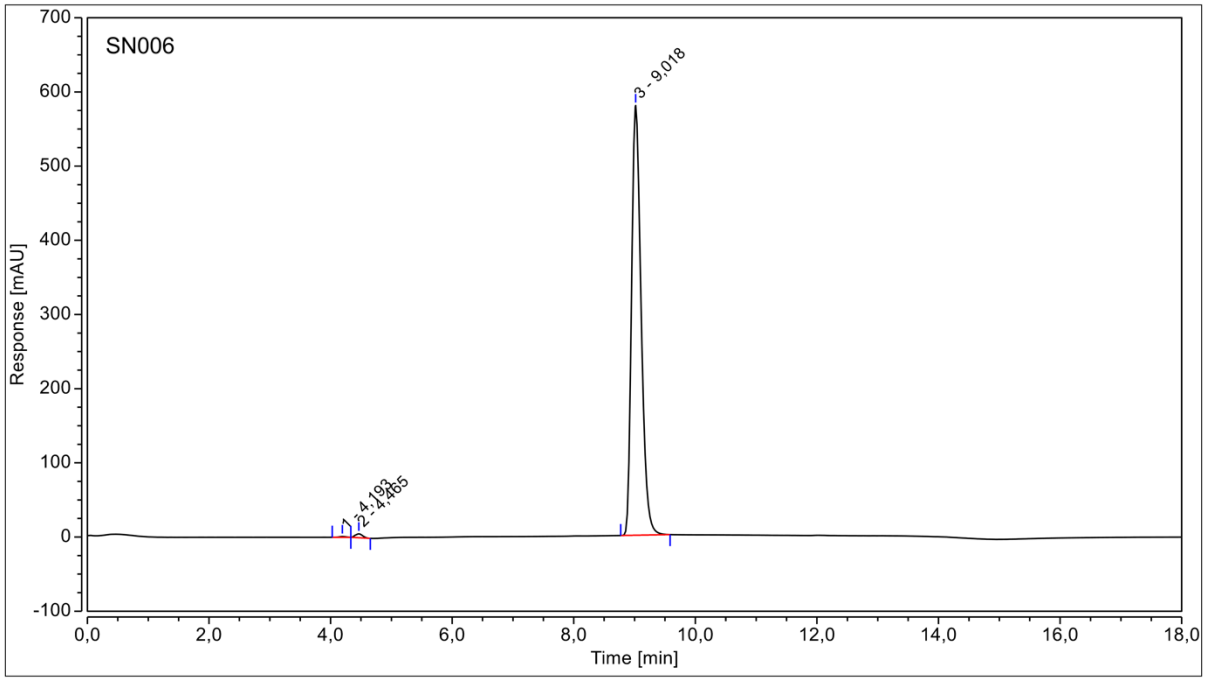

Figure S1.20: HPLC chromatogram of SN006. A retention time of 9.018 min with a relative purity of 99.18 % was determined for the compound at 280 nm detection wavelength.

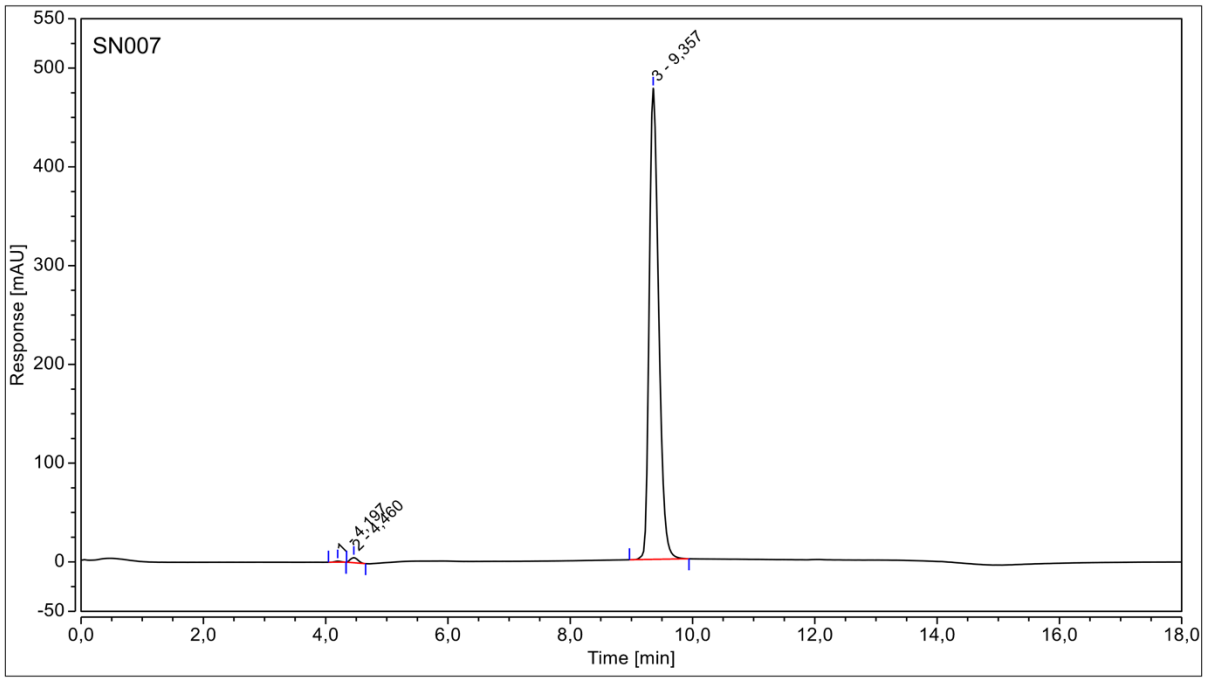

Figure S1.21: HPLC chromatogram of SN007. A retention time of 9.357 min with a relative purity of 99.00 % was determined for the compound at 280 nm detection wavelength.

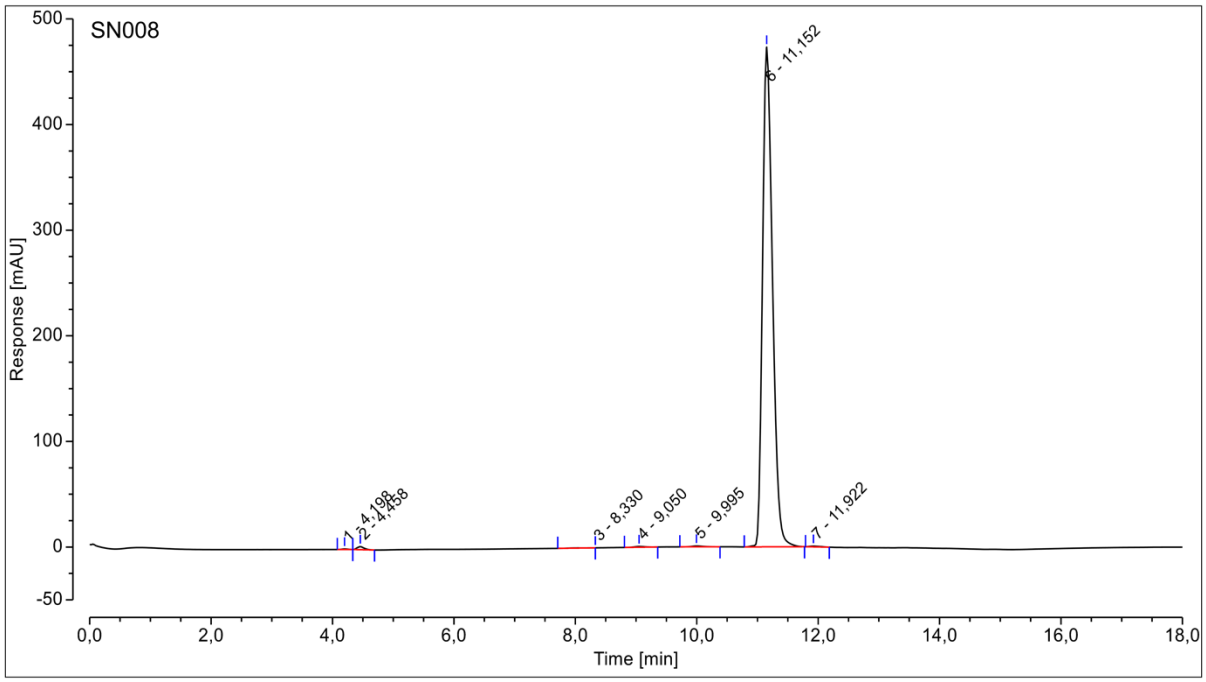

Figure S1.22: HPLC chromatogram of SN008. A retention time of 11.152 min with a relative purity of 98.96 % was determined for the compound at 254 nm detection wavelength.

Table S1.1: Results of the purity assessment of the analyzed fragments using HPLC-UV. The retention times and relative purities were determined and calculated at the wavelength shown

compound	retention time [min]	purity [%]	detection wavelength [nm]
CA001	6.462	99.72	254
CA002	8.753	98.75	254
CA003	7.897	99.44	254
CA004	10.767	99.81	254
CA005	10.618	99.29	254
EO001	10.927	92.99	254
EO002	n.a.	n.a.	n.a.
EO003	6.730	99.12	254
VS001	n.a.	n.a.	n.a.
VS002	8.832	95.50	280
VS003	9.795	99.04	218
VS004	9.882	98.67	254
SN001	8.013	98.36	218
SN002	6.070	99.38	254
SN003	9.743	99.36	254
SN004	11.970	96.73	254
SN005	10.240	99.54	254
SN006	9.018	99.18	280
SN007	9.357	99.00	280
SN008	11.152	98.96	254

n.a., not available

2. Turbidimetric Solubility Assay

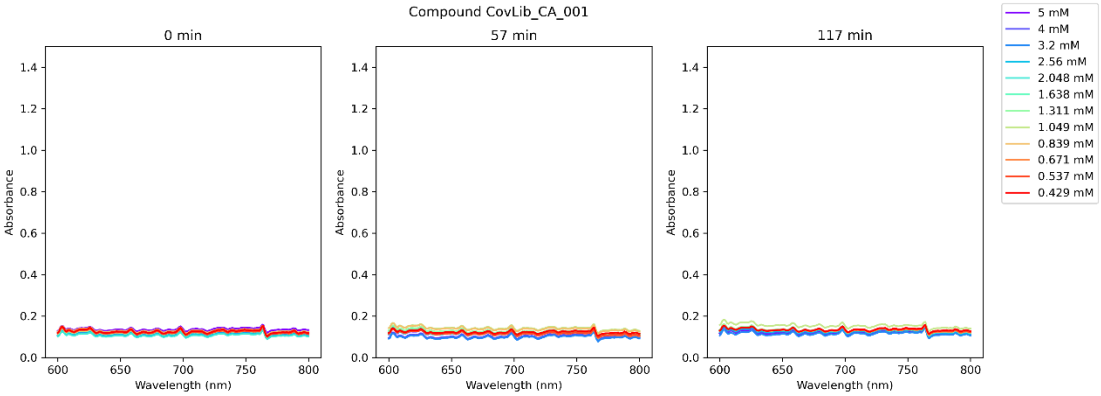

Figure S2.1: Spectra of the Turbidimetric solubility measurement of fragment CA001.

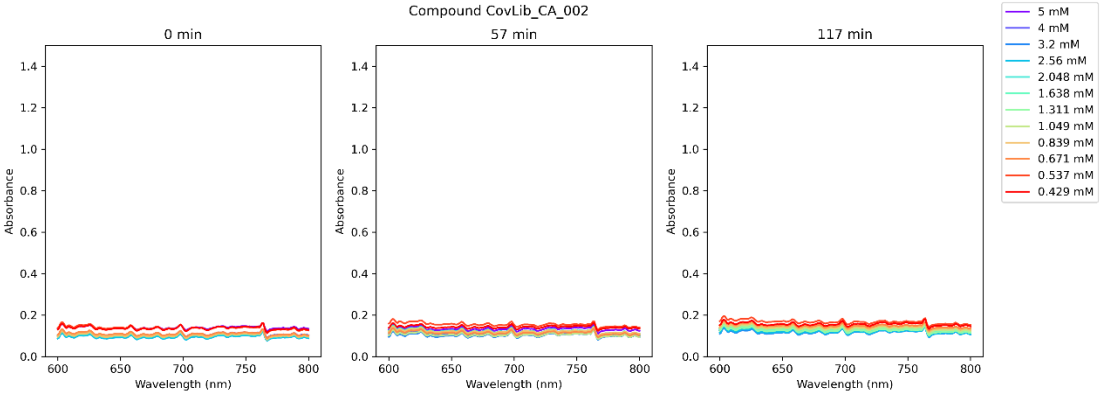

Figure S2.2: Spectra of the Turbidimetric solubility measurement of fragment CA002.

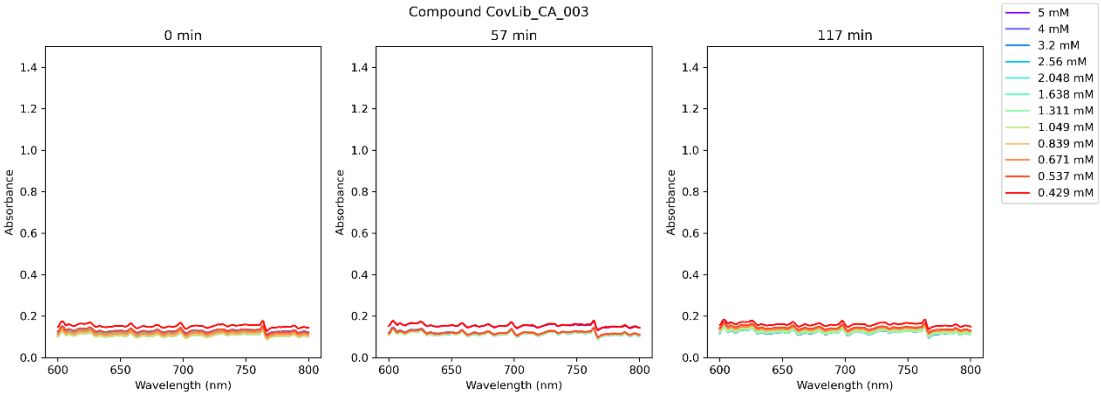

Figure S2.3: Spectra of the Turbidimetric solubility measurement of fragment CA003.

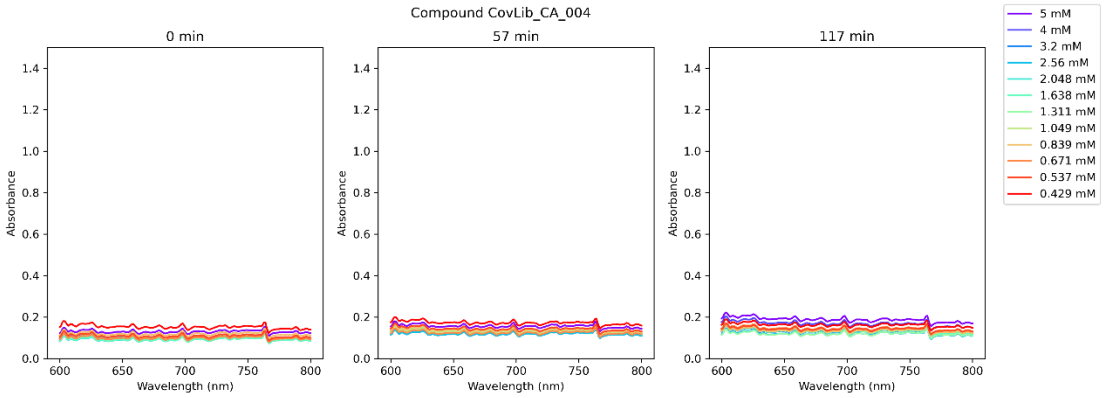

Figure S2.4: Spectra of the Turbidimetric solubility measurement of fragment CA004.

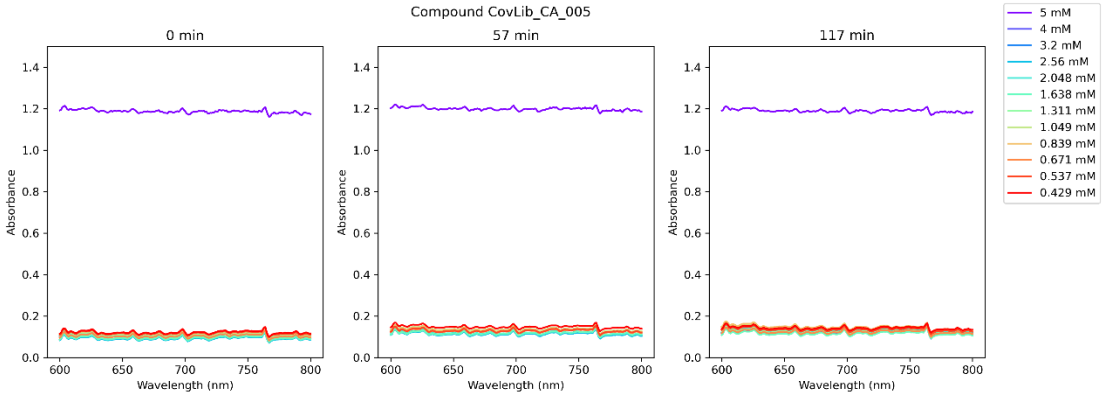

Figure S2.5: Spectra of the Turbidimetric solubility measurement of fragment CA005.

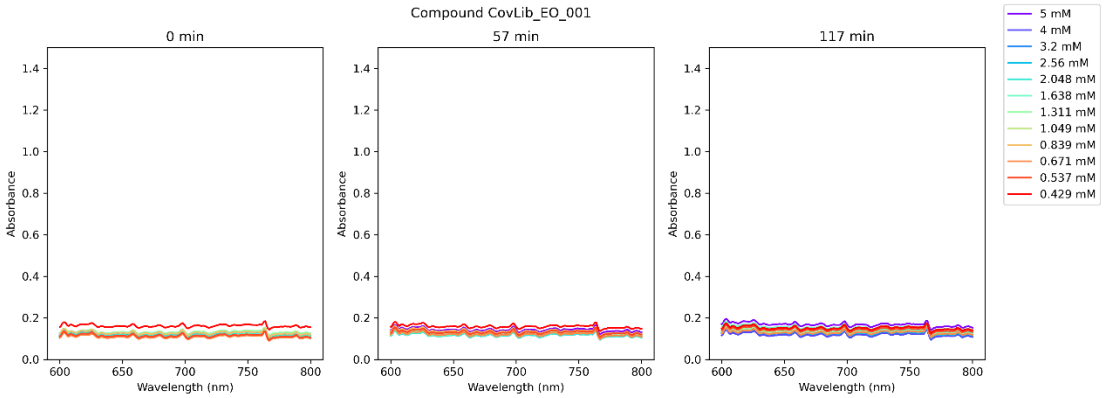

Figure S2.6: Spectra of the Turbidimetric solubility measurement of fragment EO001.

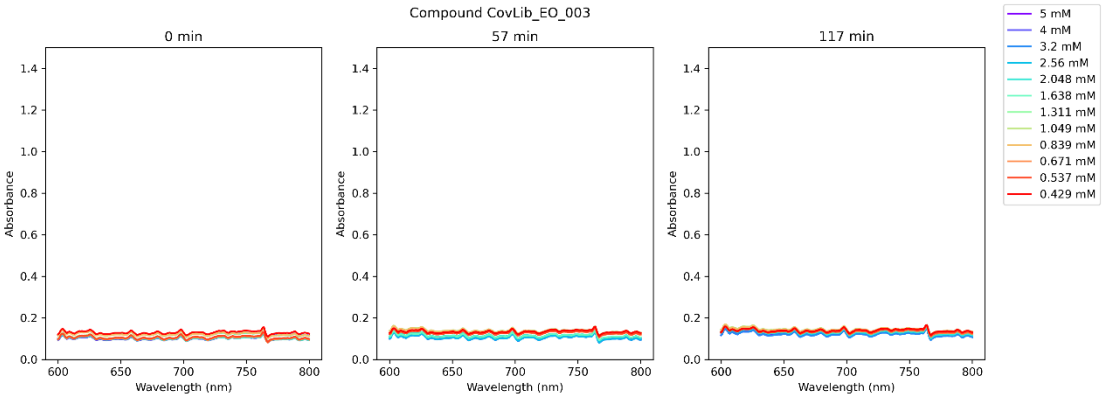

Figure S2.7: Spectra of the Turbidimetric solubility measurement of fragment EO003.

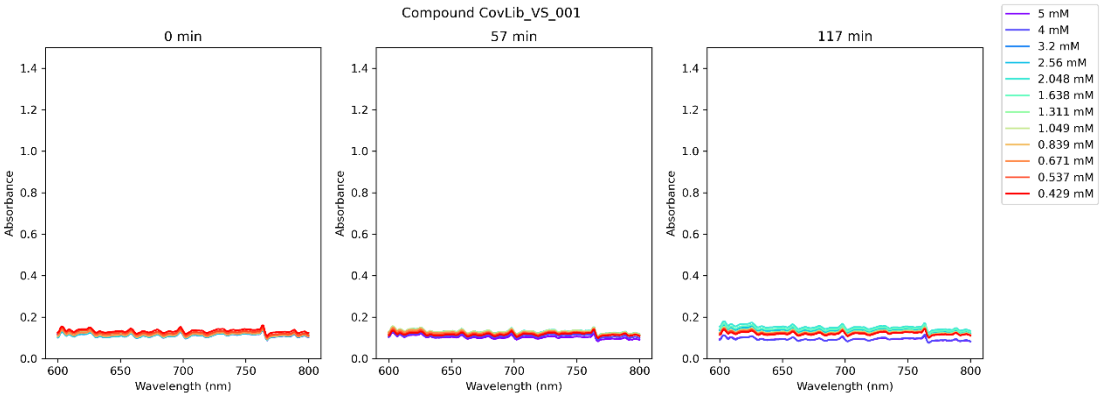

Figure S2.8: Spectra of the Turbidimetric solubility measurement of fragment VS001.

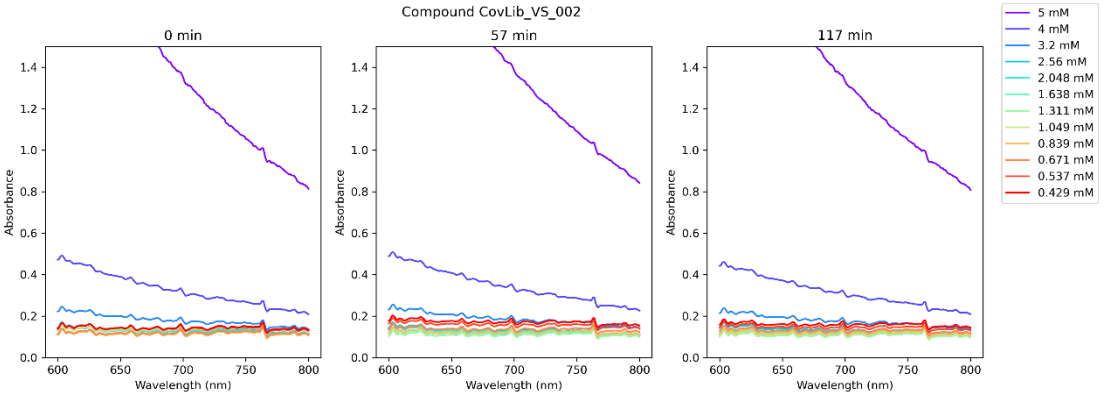

Figure S2.9: Spectra of the Turbidimetric solubility measurement of fragment VS002.

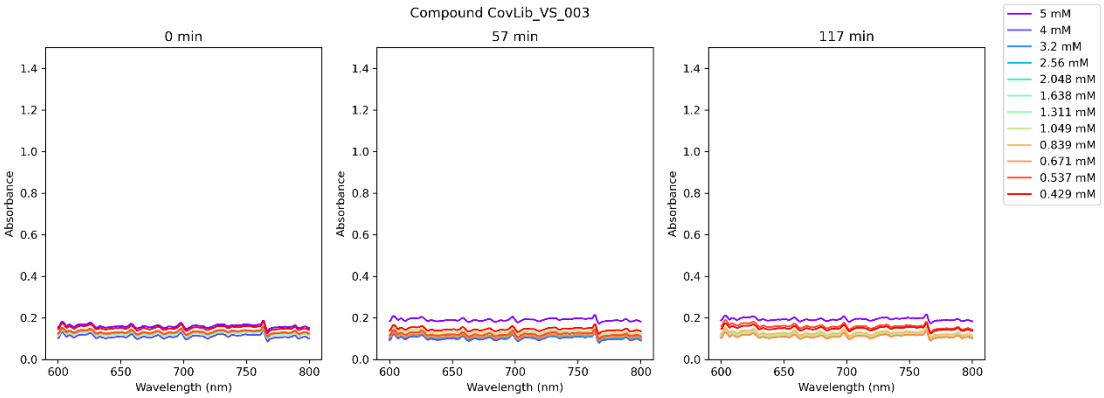

Figure S2.10: Spectra of the Turbidimetric solubility measurement of fragment VS003.

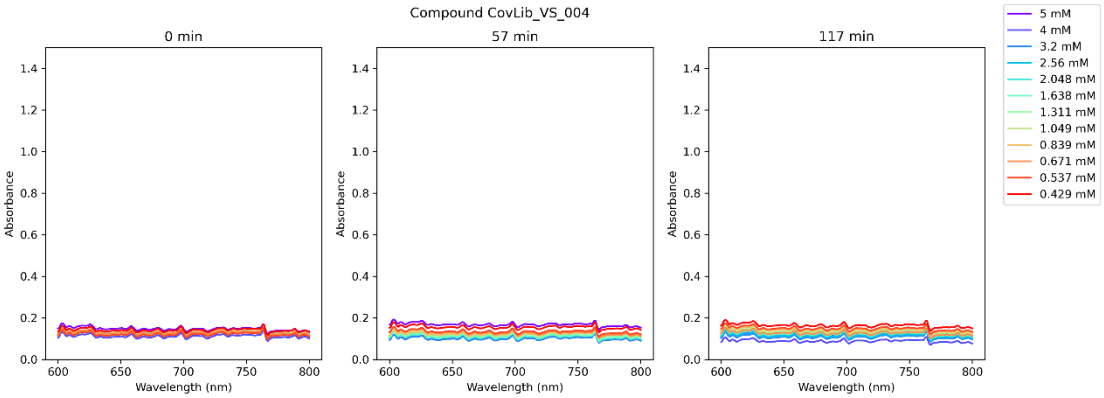

Figure S2.11: Spectra of the Turbidimetric solubility measurement of fragment VS004.

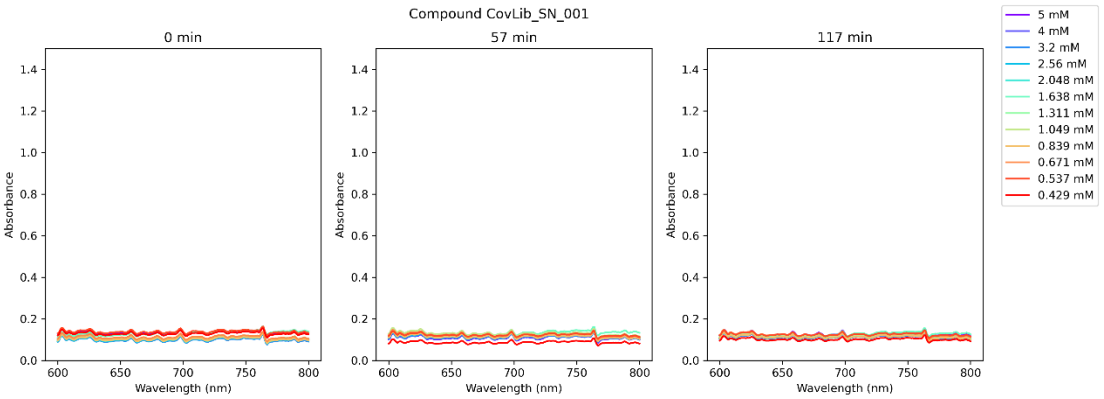

Figure S2.12: Spectra of the Turbidimetric solubility measurement of fragment SN001.

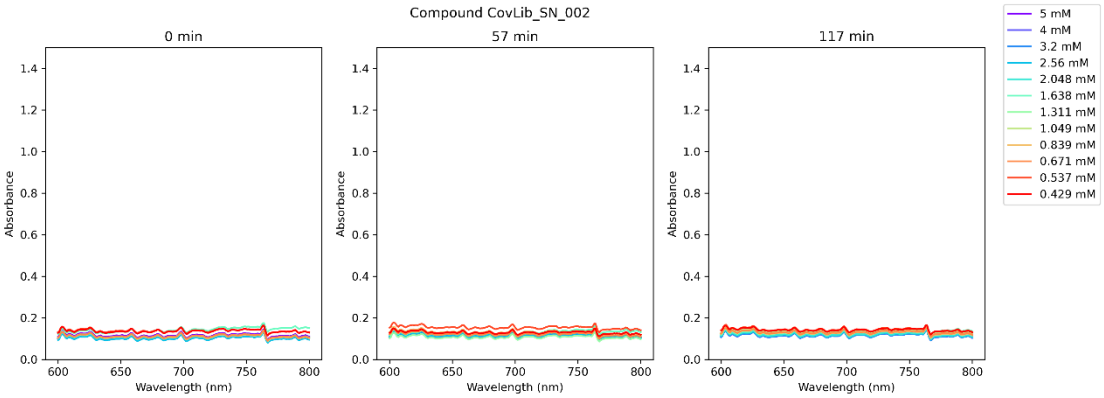

Figure S2.13: Spectra of the Turbidimetric solubility measurement of fragment SN002.

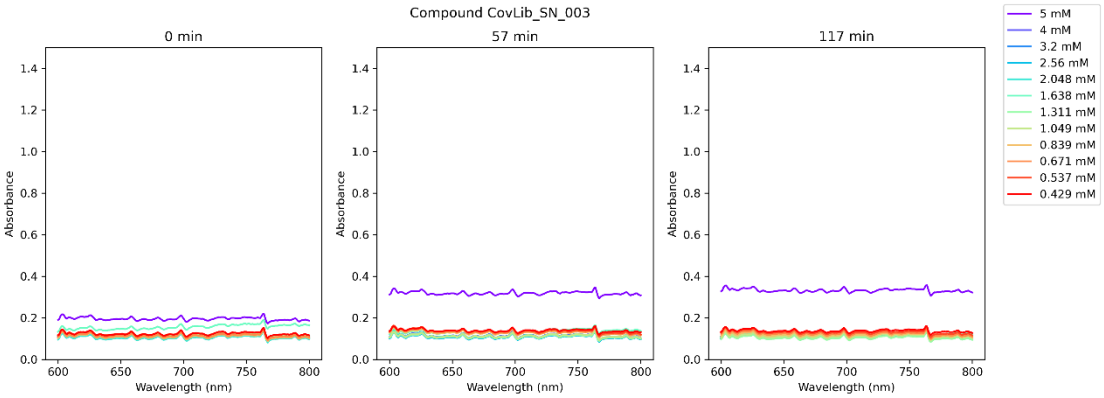

Figure S2.14: Spectra of the Turbidimetric solubility measurement of fragment SN003.

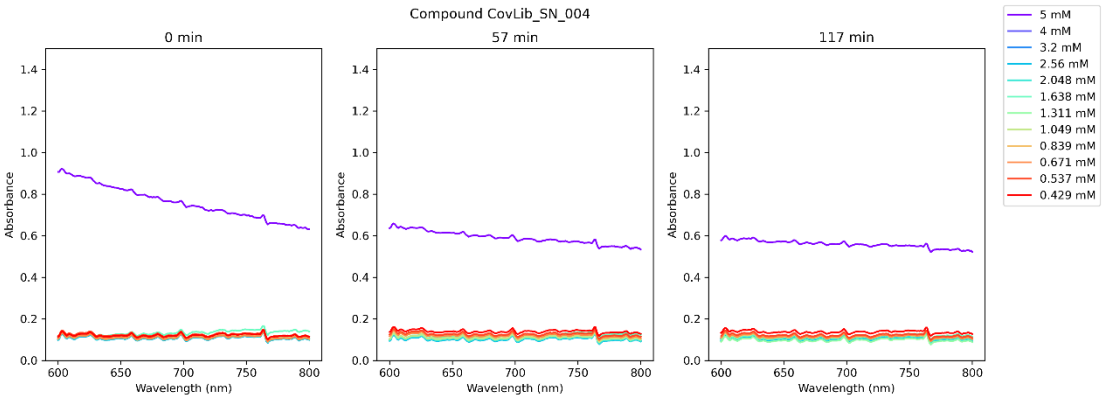

Figure S2.15: Spectra of the Turbidimetric solubility measurement of fragment SN004.

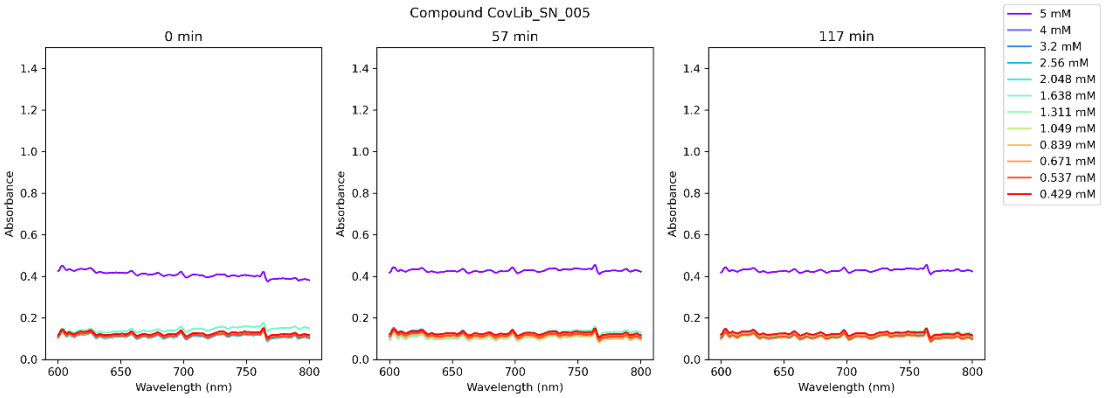

Figure S2.16: Spectra of the Turbidimetric solubility measurement of fragment SN005.

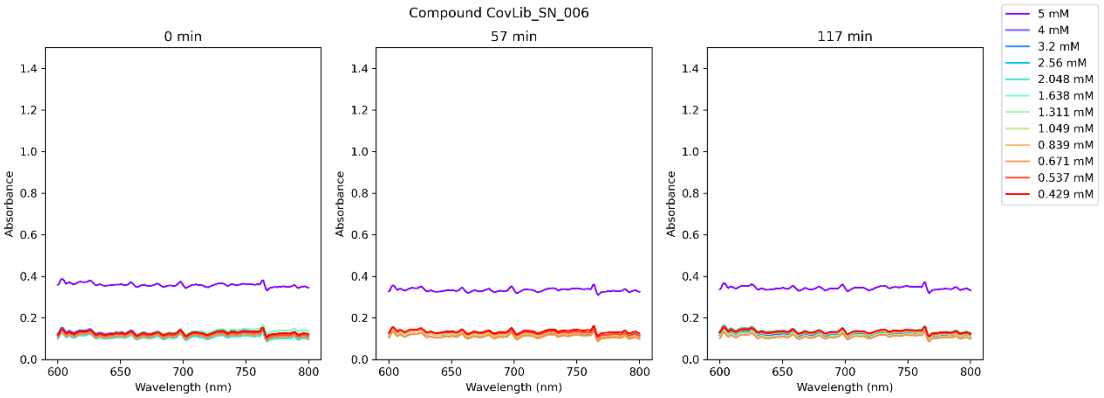

Figure S2.17: Spectra of the Turbidimetric solubility measurement of fragment SN006.

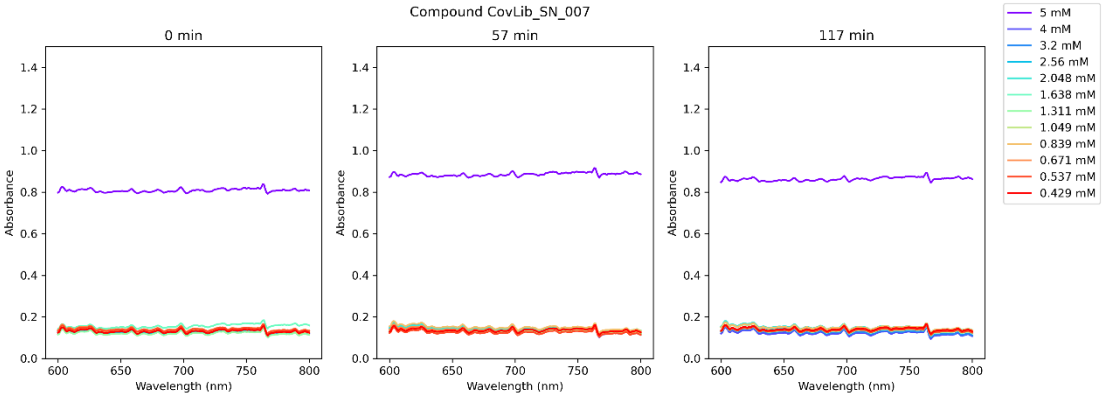

Figure S2.18: Spectra of the Turbidimetric solubility measurement of fragment SN007.

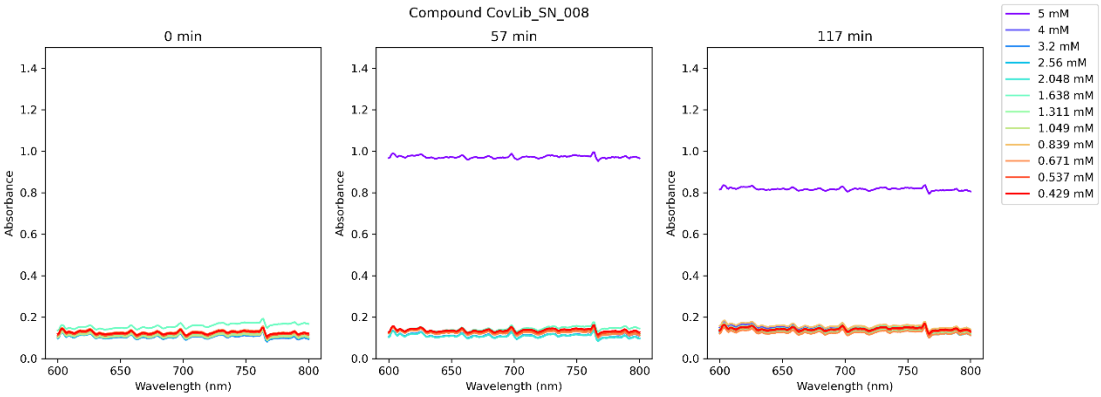

Figure S2.19: Spectra of the Turbidimetric solubility measurement of fragment SN008.

3. DTNB Assay

Table S3.1: Results and parameters of the second-order kinetic fit of the first measurement of the DTNB assay

measurement 1							
compound	k_2 [$M^{-1}s^{-1}$]	error	t_d [min]	error	$[B_0]$ [µM]	error	$[A_0]$ [µM]
Iodoacetamide	3.6	0.0	0.69	0.25	40	0	100
CA001	0.0017	0.0032	0	0	50	0	103
CA002	0.041	0.007	0	0	50	0	101
CA003	0.0022	0.0059	0	0	50	0	100
CA004	0.034	0.001	0	0	50	0	101
CA005	0.052	0.002	0	0	50	0	101
EO001	0.044	0.001	0	0	50	0	101
EO002	n.a.	n.a.	n.a.	n.a.	n.a.	n.a.	n.a.
EO003	0.039	0.001	0	0	50	0	101
VS001	0.036	0.003	0	0	50	0	99
VS002	2.3	0.055	0	0	44	0	100
VS003	0.022	0.001	0	0	50	0	101
VS004	-0.0022	0.0027	0	0	50	0	98
SN001	3.0	0.0	0	0	34	0	100
SN002	0.14	0.00	0	0	50	0	100
SN003	0.044	0.002	0	0	50	0	99
SN004	0.0089	0.0040	0	0	50	0	101
SN005	0.063	0.001	0	0	50	0	100
SN006	25	0	3.5	0.1	50	0	100
SN007	62	3	4.1	0.2	48	0	100
SN008	0.032	0.001	0	0	50	0	100

n.a., not available

Table S3.2: Results and parameters of the second-order kinetic fit of the second measurement of the DTNB assay

	measurement 2						
compound	k_2 [$M^{-1}s^{-1}$]	error	t_d [min]	error	$[B_0]$ [µM]	error	$[A_0]$ [µM]
Iodoacetamide	0.69	0.25	2.4	0.3	42	0	100
CA001	0.021	0.003	0	0	50	0	101
CA002	0.011	0.006	0	0	50	0	100
CA003	0.0088	0.0023	0	0	50	0	101
CA004	0.029	0.002	0	0	50	0	99
CA005	0.048	0.002	0	0	50	0	99
EO001	0.069	0.000	0	0	50	0	989
EO002	n.a.	n.a.	n.a.	n.a.	n.a.	n.a.	n.a.
EO003	0.031	0.002	0	0	50	0	99
VS001	0.018	0.002	0	0	50	0	97
VS002	2.7	0.1	0	0	42	0	100
VS003	0.024	0.002	0	0	50	0	99
VS004	0.042	0.002	0	0	50	0	98
SN001	3.2	0.1	0	0	43	0	100
SN002	0.092	0.001	0	0	50	0	99
SN003	0.031	0.001	0	0	50	0	99
SN004	0.098	0.001	0	0	50	0	99
SN005	0.026	0.001	0	0	50	0	99
SN006	26	0	3.7	0.2	50	0	100
SN007	64	11	4.2	0.9	49	0	100
SN008	0.025	0.001	0	0	50	0	99

n.a., not available

Table S3.3: Results and parameters of the second-order kinetic fit of the third measurement of the DTNB assay. Calculated mean value of the results of measurements one to three of the DTNB assay

	measurement 3							mean	
compound	k_2 [$M^{-1}s^{-1}$]	error	t_d [min]	error	[B_0] [µM]	error	[A_0] [µM]	k_2 [$M^{-1}s^{-1}$]	error
Iodoacetamide	3.6	0.0	2.5	0.3	42	0	100	2.6	0.1
CA001	0.022	0.002	0	0	50	0	100	0.015	0.002
CA002	0.058	0.005	0	0	50	0	99	0.037	0.004
CA003	0.035	0.001	0	0	50	0	98	0.015	0.002
CA004	0.026	0.001	0	0	50	0	100	0.030	0.001
CA005	0.048	0.002	0	0	50	0	99	0.049	0.001
EO001	0.12	0.00	0	0	50	0	98	0.076	0.000
EO002	n.a.	n.a.	n.a.	n.a.	n.a.	n.a.	n.a.	n.a.	n.a.
EO003	0.021	0.002	0	0	50	0	99	0.030	0.001
VS001	0.038	0.001	0	0	50	0	97	0.031	0.001
VS002	2.8	0.1	0	0	42	0	100	2.6	0.0
VS003	0.0088	0.0046	0	0	50	0	99	0.018	0.002
VS004	0.035	0.001	0	0	50	0	98	0.025	0.001
SN001	2.4	0.1	0	0	34	0	100	2.9	0.0
SN002	0.084	0.001	0	0	50	0	99	0.11	0.00
SN003	-0.014	0.005	0	0	50	0	98	0.020	0.002
SN004	0.15	0.00	0	0	50	0	98	0.086	0.001
SN005	0.026	0.001	0	0	50	0	99	0.038	0.001
SN006	26	1	3.9	0.2	50	0	100	26	0
SN007	68	2	4.2	0.2	49	0	100	65	4
SN008	0.025	0.001	0	0	50	0	98	0.027	0.001

n.a., not available

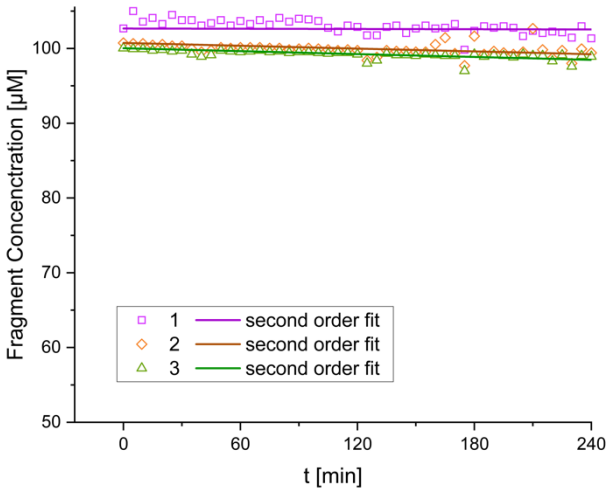

Figure S3.1: Time dependent concentration of fragment CA001 in the DTNB assay.

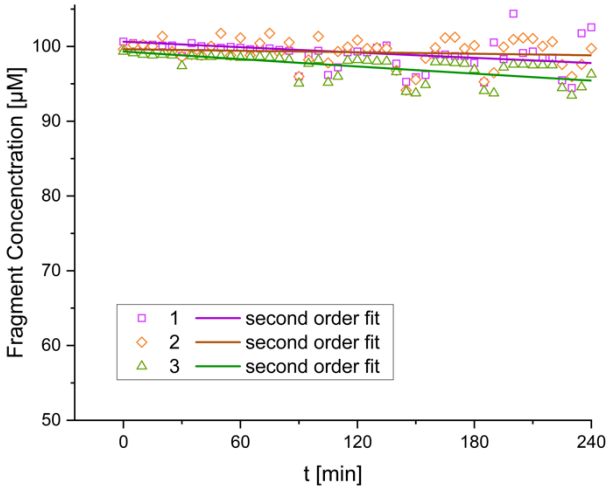

Figure S3.2: Time dependent concentration of fragment CA002 in the DTNB assay.

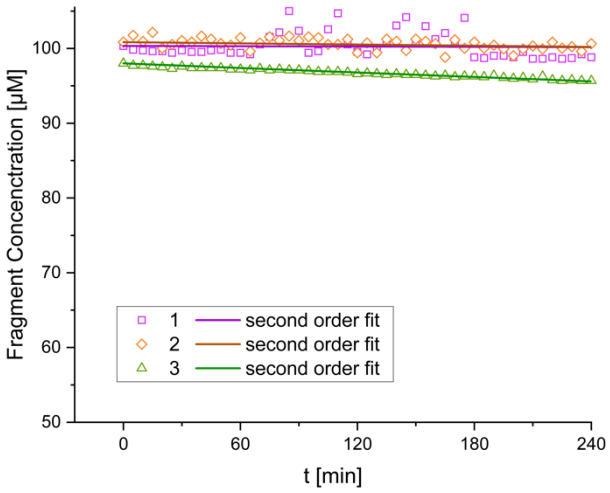

Figure S3.3: Time dependent concentration of fragment CA003 in the DTNB assay.

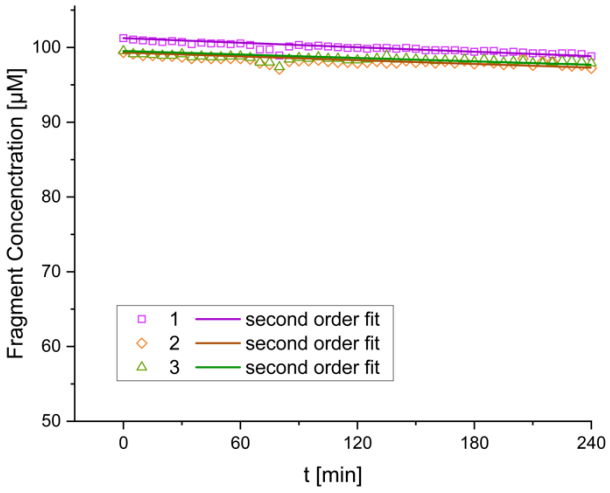

Figure S3.4: Time dependent concentration of fragment CA004 in the DTNB assay.

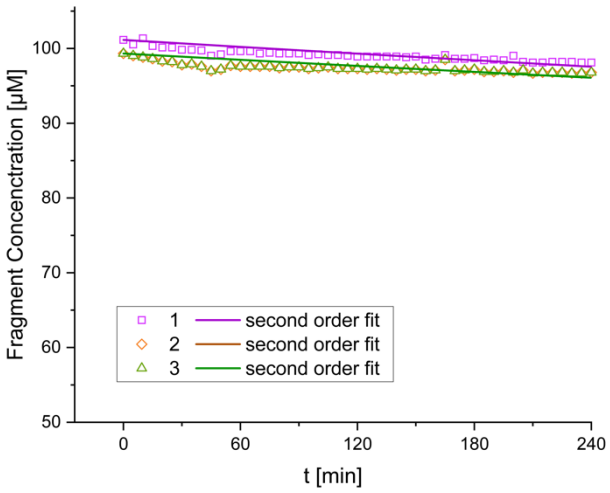

Figure S3.5: Time dependent concentration of fragment CA005 in the DTNB assay.

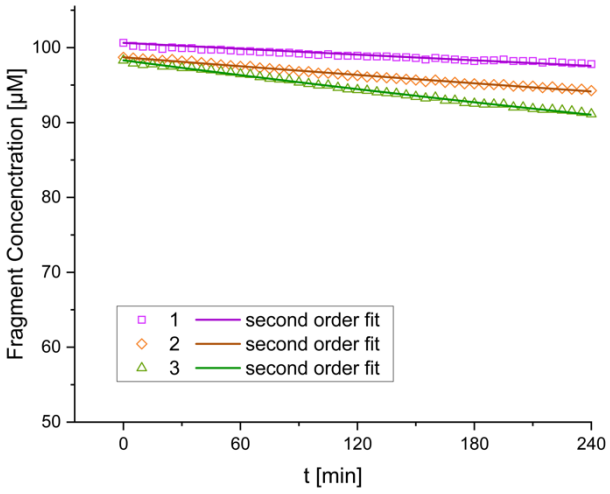

Figure S3.6: Time dependent concentration of fragment EO001 in the DTNB assay.

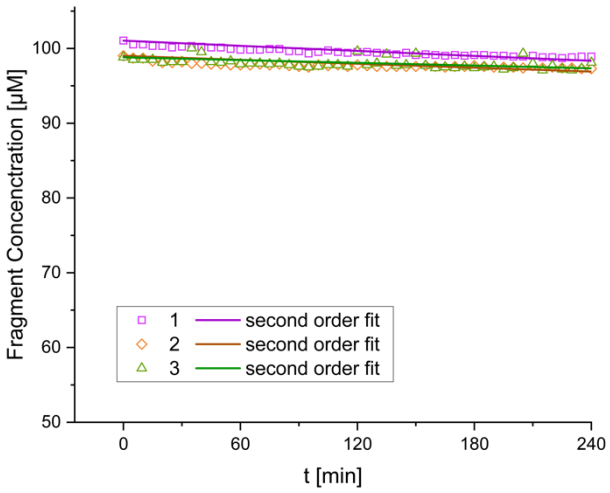

Figure S3.7: Time dependent concentration of fragment EO003 in the DTNB assay.

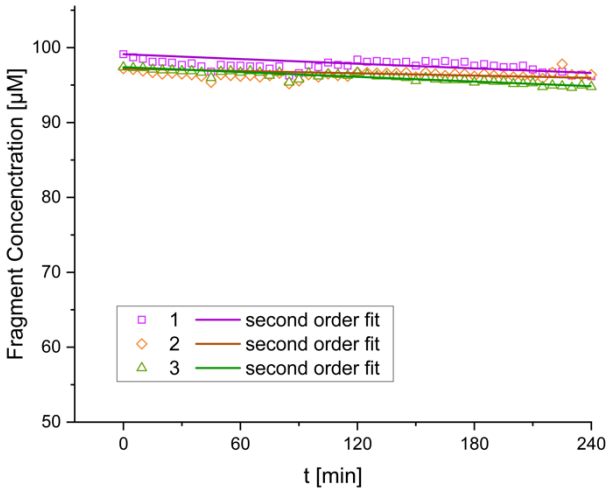

Figure S3.8: Time dependent concentration of fragment VS001 in the DTNB assay.

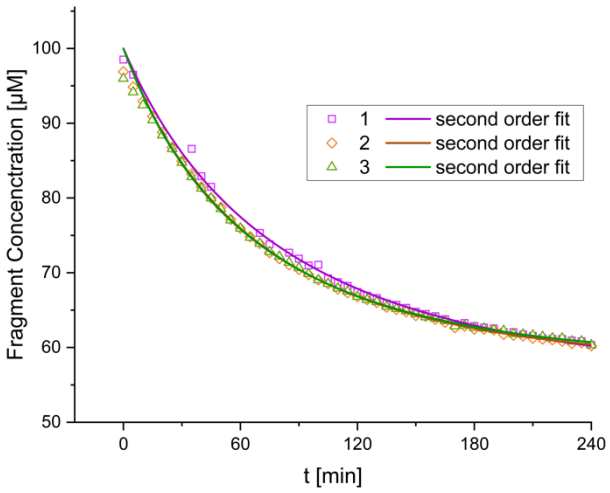

Figure S3.9: Time dependent concentration of fragment VS002 in the DTNB assay.

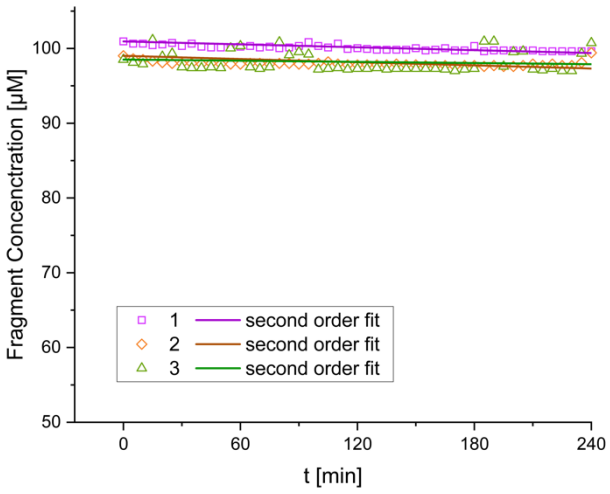

Figure S3.10: Time dependent concentration of fragment VS003 in the DTNB assay.

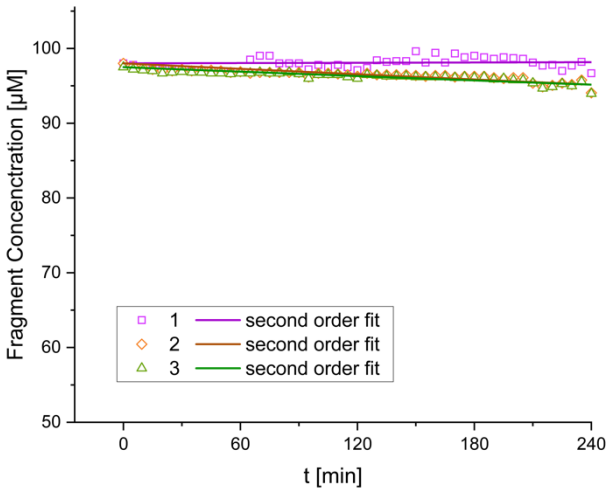

Figure S3.11: Time dependent concentration of fragment VS004 in the DTNB assay.

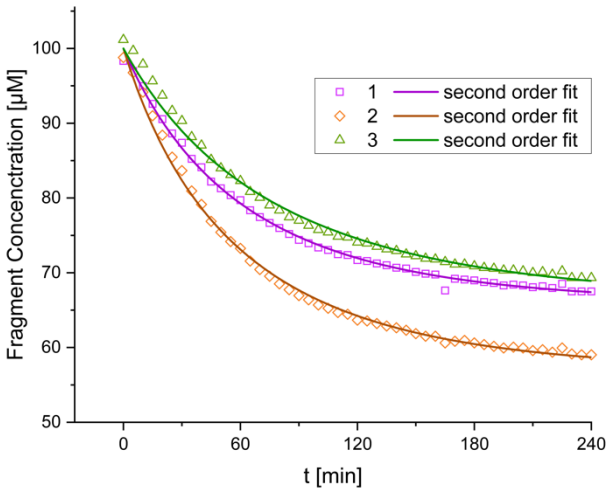

Figure S3.12: Time dependent concentration of fragment SN001 in the DTNB assay.

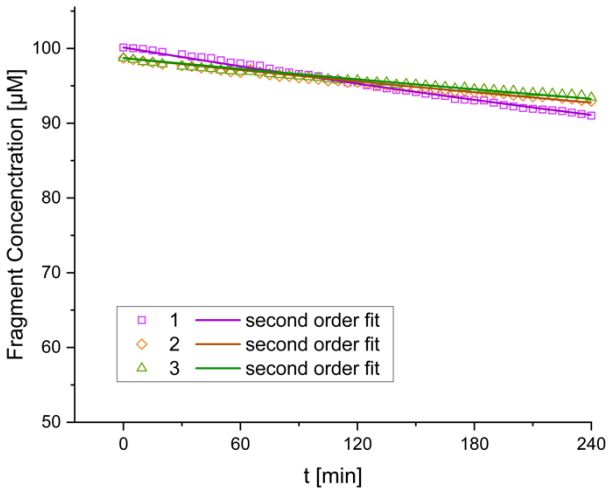

Figure S3.13: Time dependent concentration of fragment SN002 in the DTNB assay.

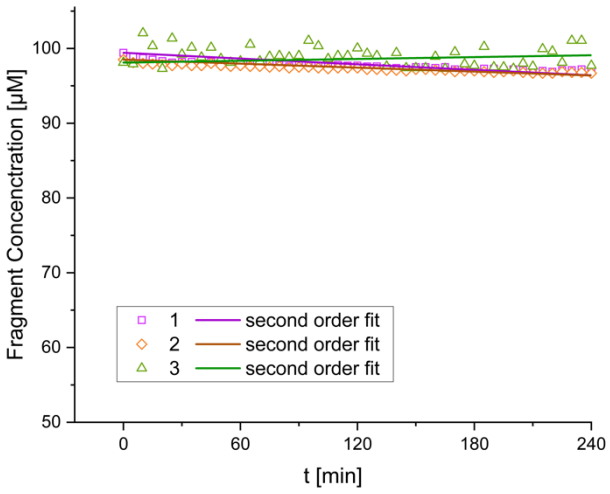

Figure S3.14: Time dependent concentration of fragment SN003 in the DTNB assay.

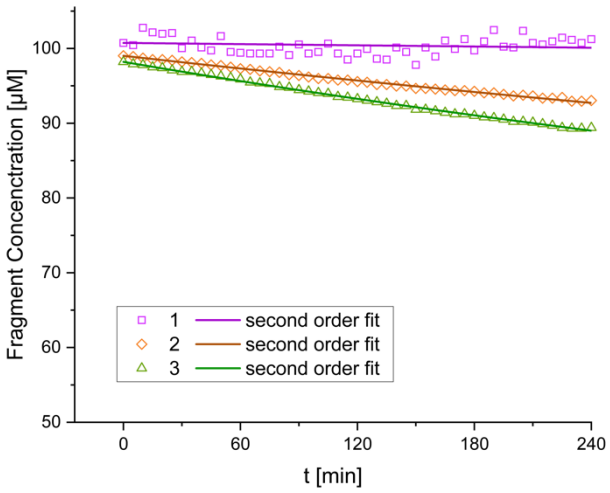

Figure S3.15: Time dependent concentration of fragment SN004 in the DTNB assay.

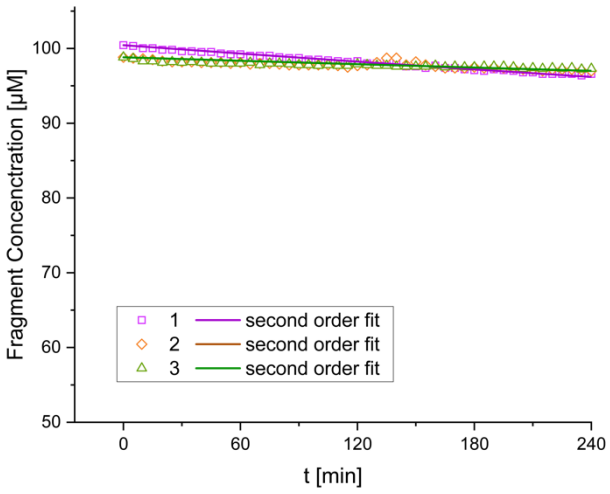

Figure S3.16: Time dependent concentration of fragment SN005 in the DTNB assay.

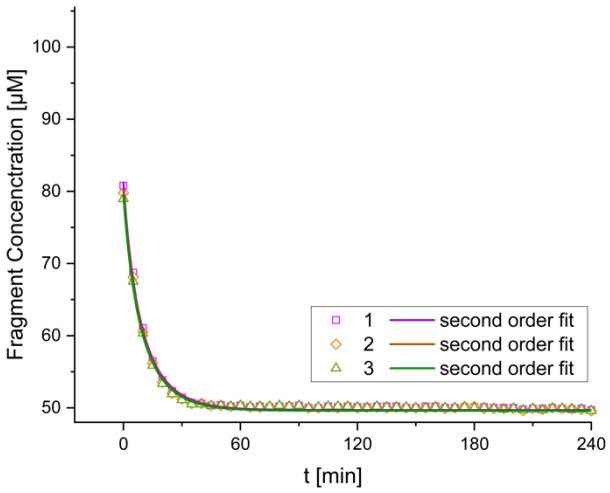

Figure S3.17: Time dependent concentration of fragment SN006 in the DTNB assay.

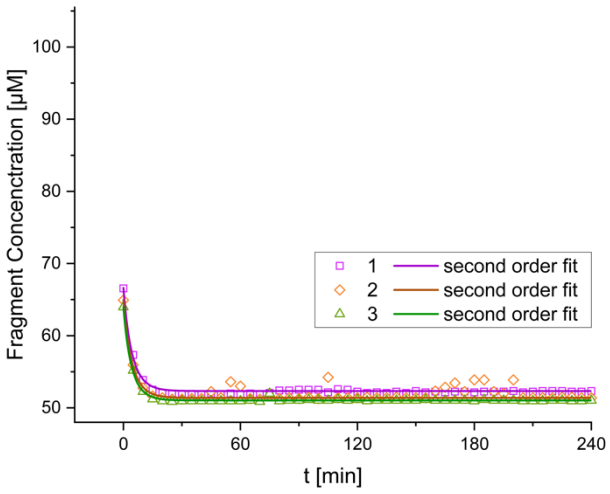

Figure S3.18: Time dependent concentration of fragment SN007 in the DTNB assay.

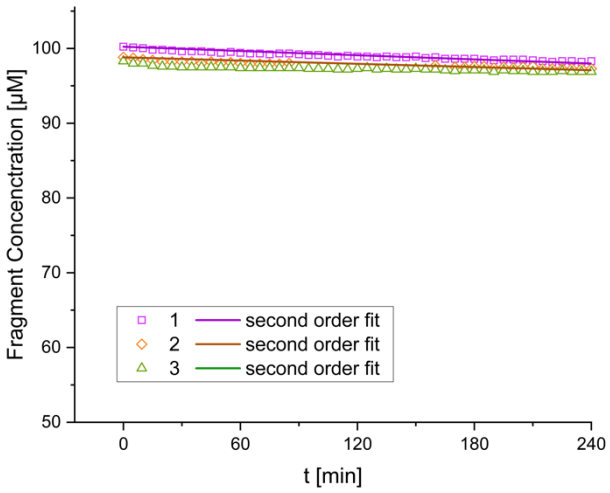

Figure S3.19: Time dependent concentration of fragment SN008 in the DTNB assay.

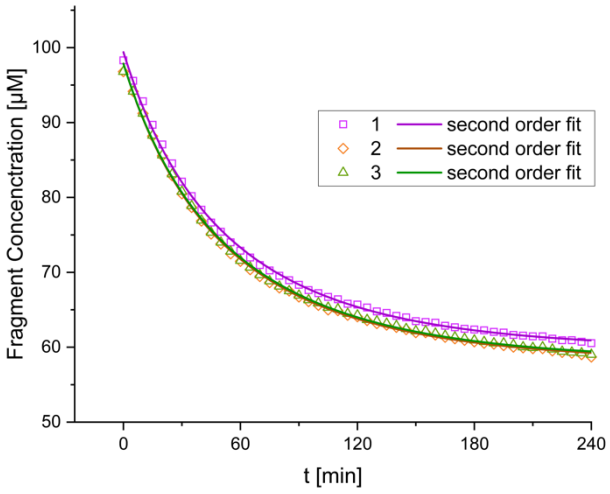

Figure S3.20: Time dependent concentration of the reference compound iodoacetamide in the DTNB assay.

4. Glutathione Assay

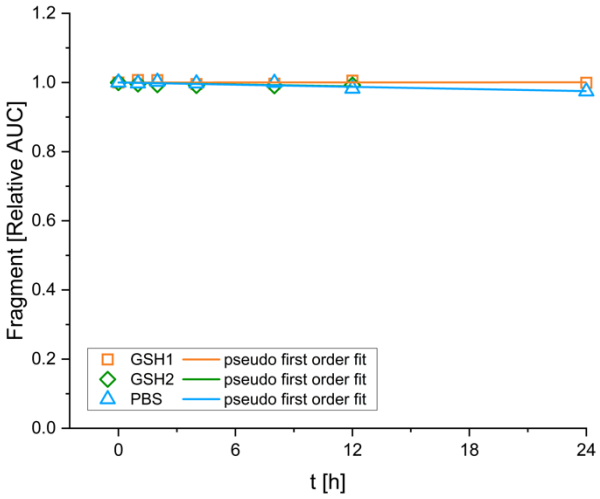

Figure S4.1: Time dependent relative AUC of fragment CA001 in the GSH assay and in PBS.

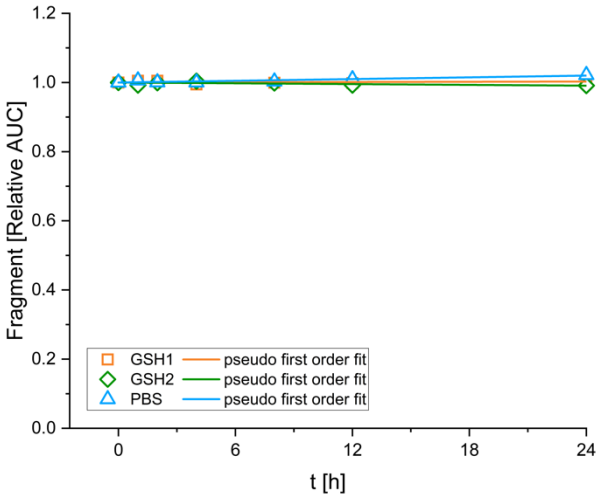

Figure S4.2: Time dependent relative AUC of fragment CA002 in the GSH assay and in PBS.

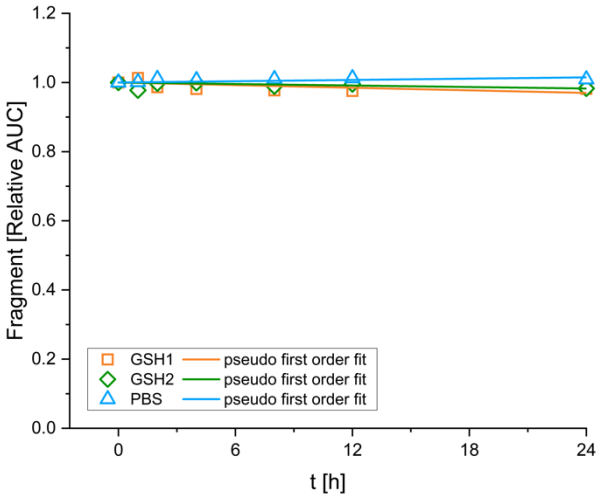

Figure S4.3: Time dependent relative AUC of fragment CA003 in the GSH assay and in PBS.

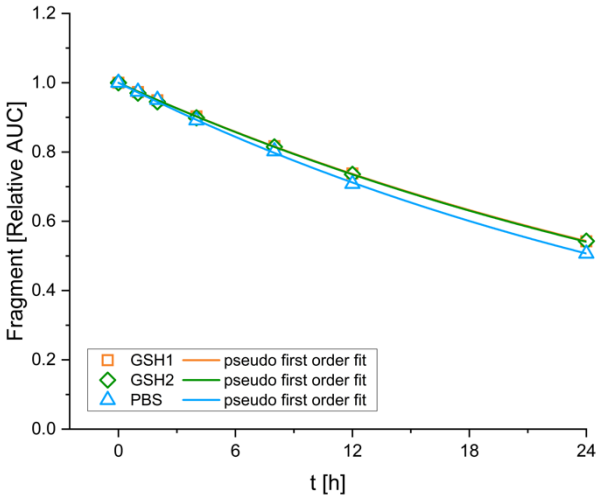

Figure S4.4: Time dependent relative AUC of fragment CA004 in the GSH assay and in PBS.

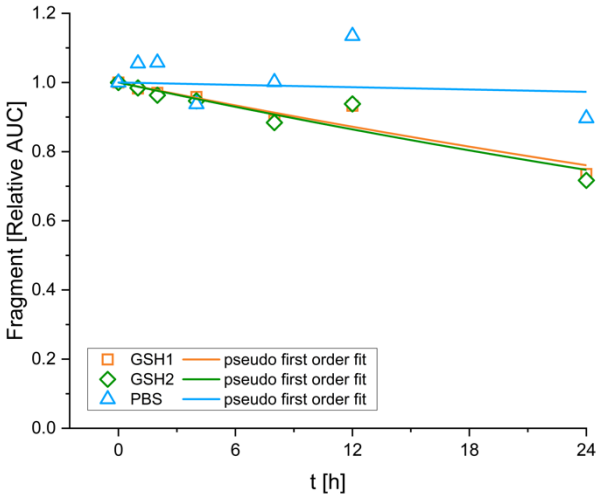

Figure S4.5: Time dependent relative AUC of fragment CA005 in the GSH assay and in PBS.

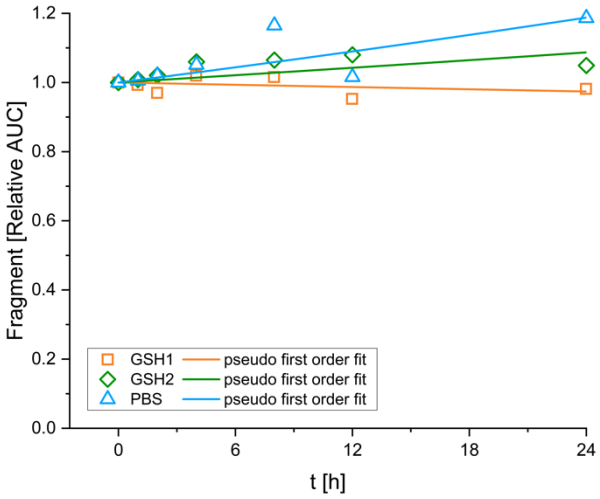

Figure S4.6: Time dependent relative AUC of fragment EO001 in the GSH assay and in PBS.

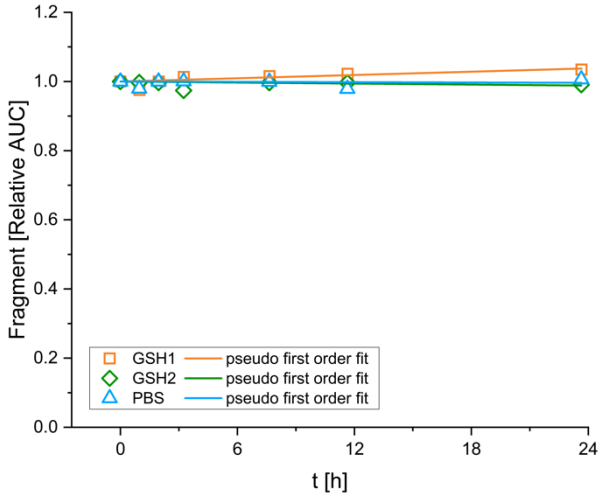

Figure S4.7: Time dependent relative AUC of fragment EO003 in the GSH assay and in PBS.

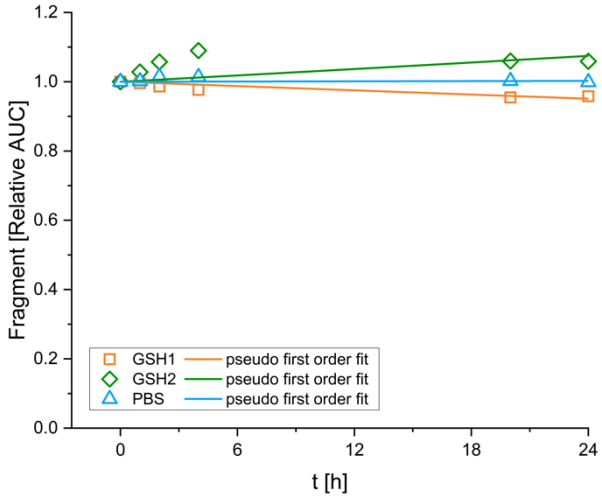

Figure S4.8: Time dependent relative AUC of fragment VS002 in the GSH assay and in PBS.

assay and in PBS.

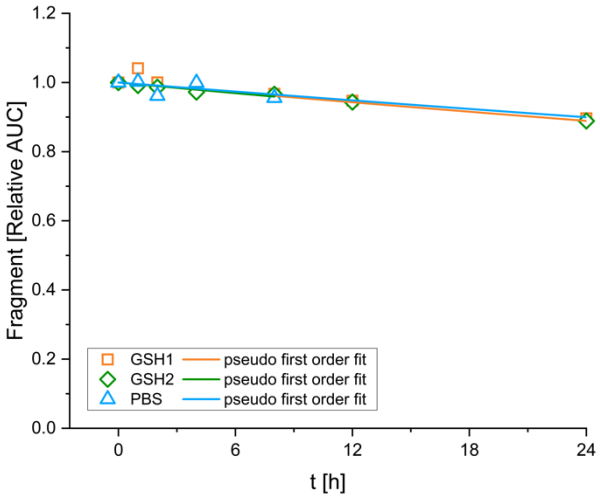

Figure S4.9: Time dependent relative AUC of fragment VS003 in the GSH assay and in PBS.

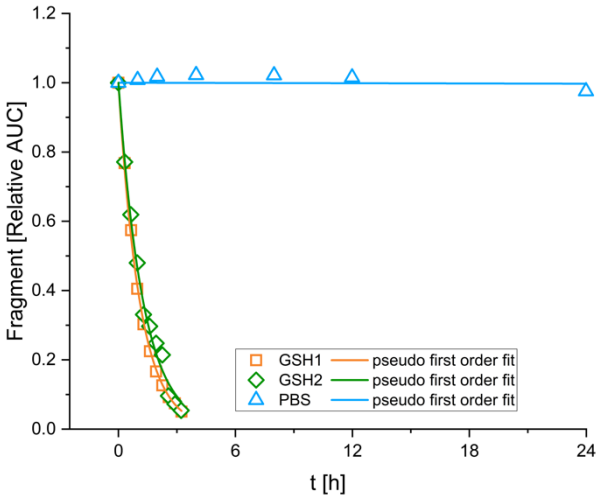

Figure S4.10: Time dependent relative AUC of fragment VS004 in the GSH assay and in PBS.

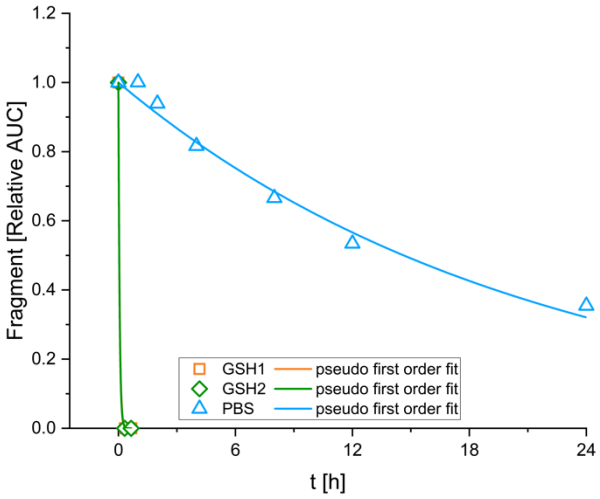

Figure S4.11: Time dependent relative AUC of fragment SN001 in the GSH assay and in PBS.

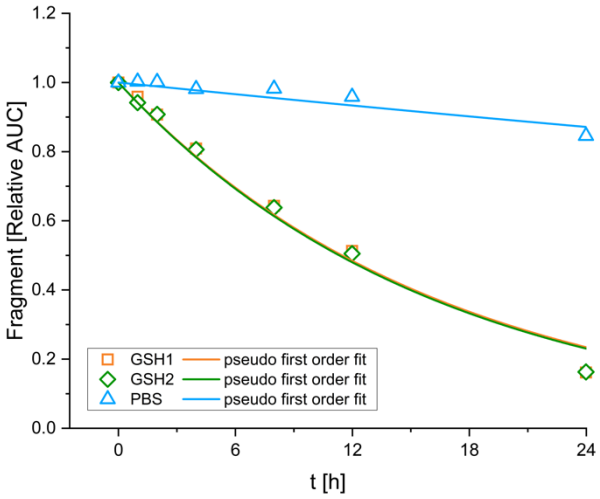

Figure S4.12: Time dependent relative AUC of fragment SN002 in the GSH assay and in PBS.

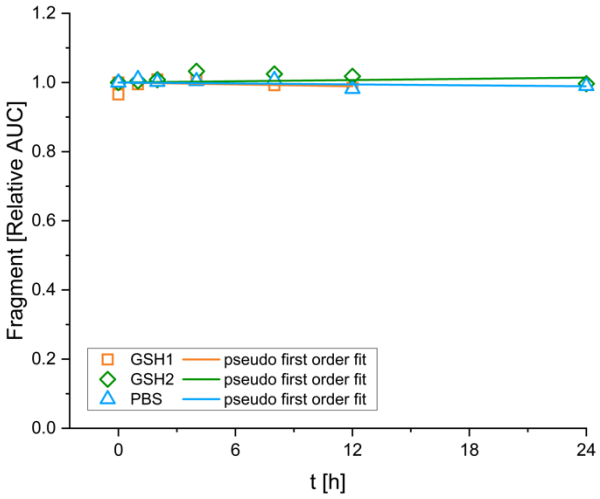

Figure S4.13: Time dependent relative AUC of fragment SN003 in the GSH assay and in PBS.

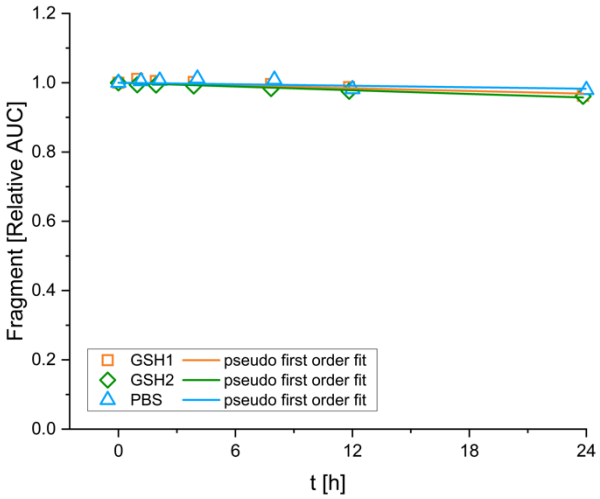

Figure S4.14: Time dependent relative AUC of fragment SN004 in the GSH assay and in PBS.

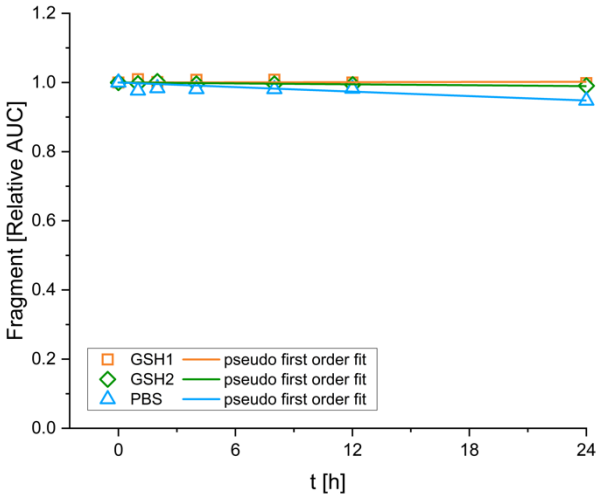

Figure S4.15: Time dependent relative AUC of fragment SN005 in the GSH assay and in PBS.

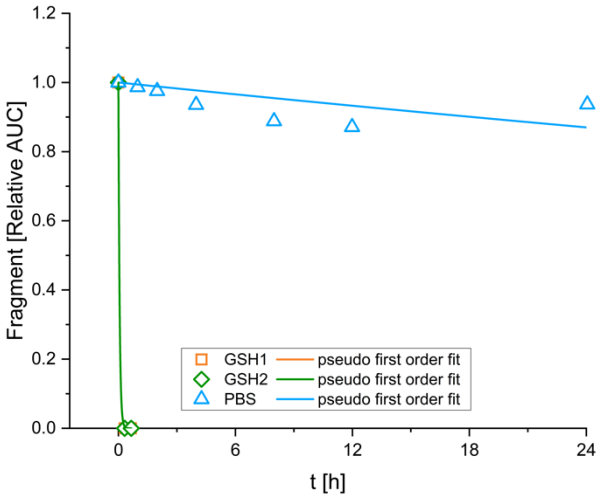

Figure S4.16 Time dependent relative AUC of fragment SN006 in the GSH assay and in PBS.

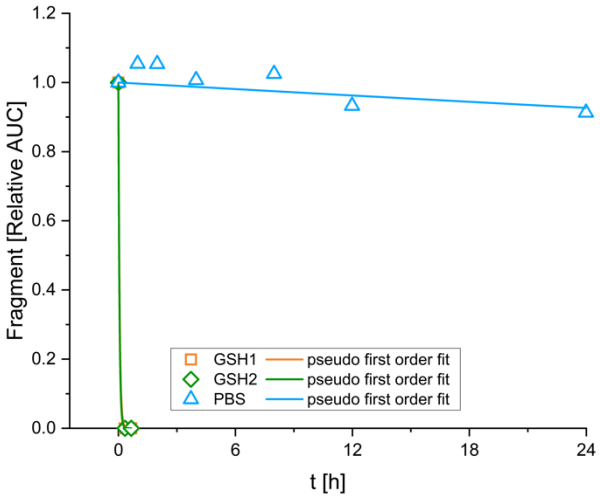

Figure S4.17: Time dependent relative AUC of fragment SN007 in the GSH assay and in PBS.

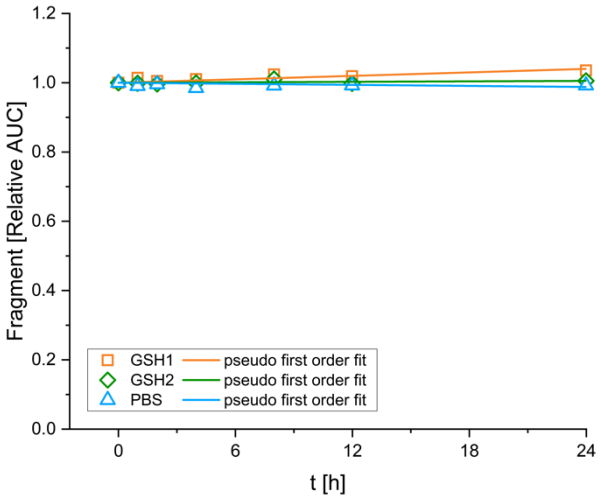

Figure S4.18: Time dependent relative AUC of fragment SN008 in the GSH assay and in PBS.

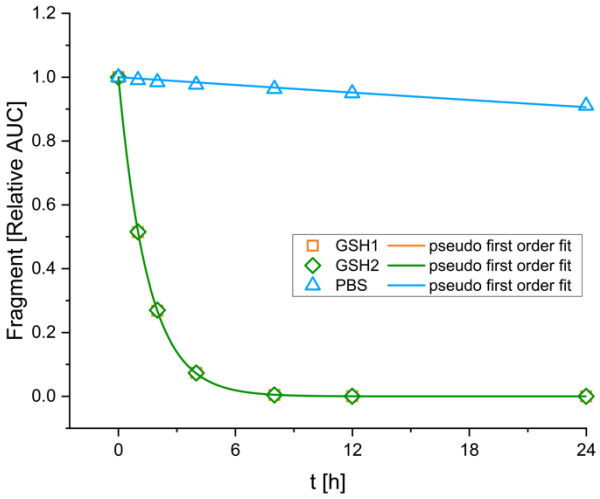

Figure S4.19: Time dependent relative AUC of the reference compound Afatinib in the GSH assay and in PBS.

5. DSF Measurements

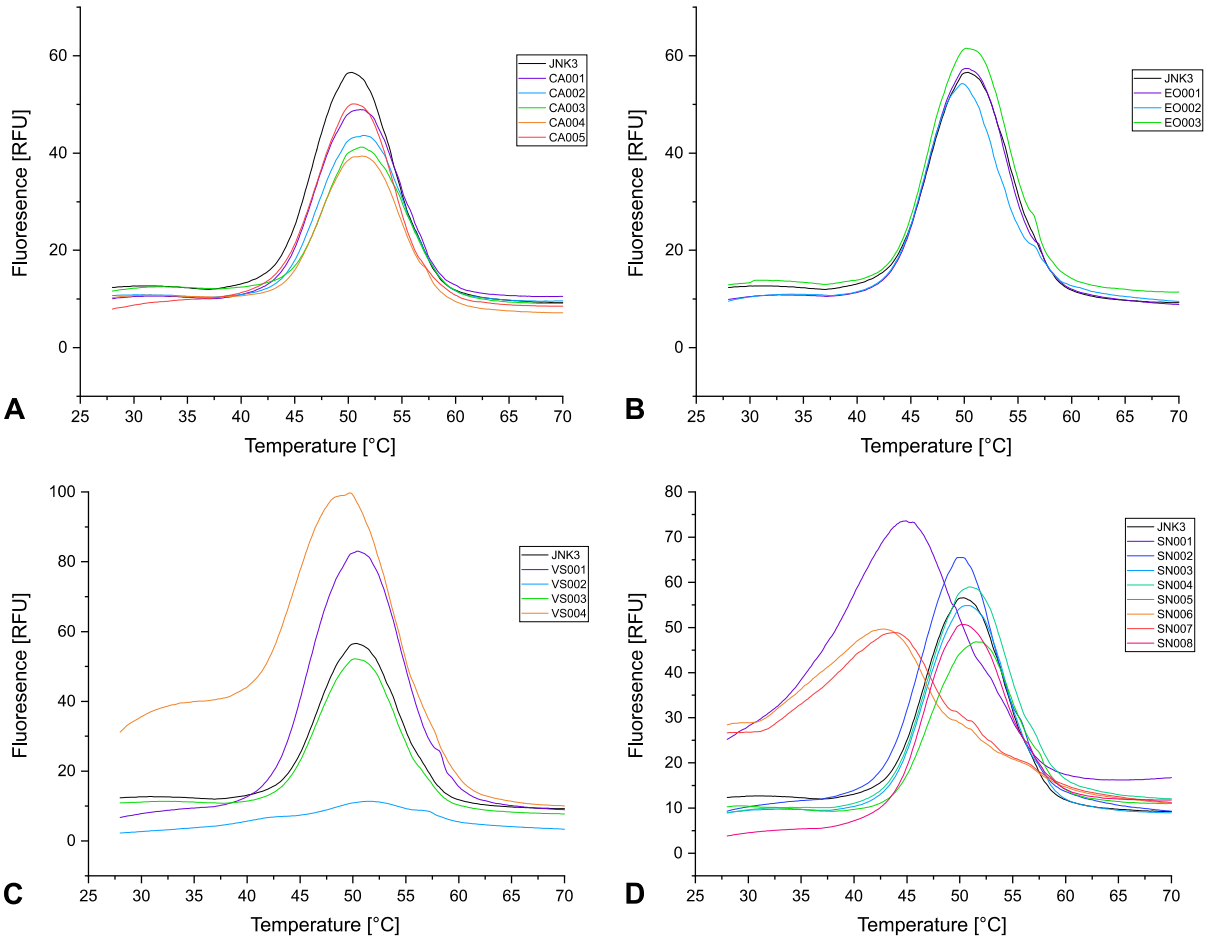

Figure S5.1: Melting curves of α-cyanoacylamides/acrylates (**A**), epoxides (**B**), vinyl sulfones (**C**), and S_NAr (**D**) fragments (1 mM) with JNK3 (8 µM protein) after 30 min incubation.

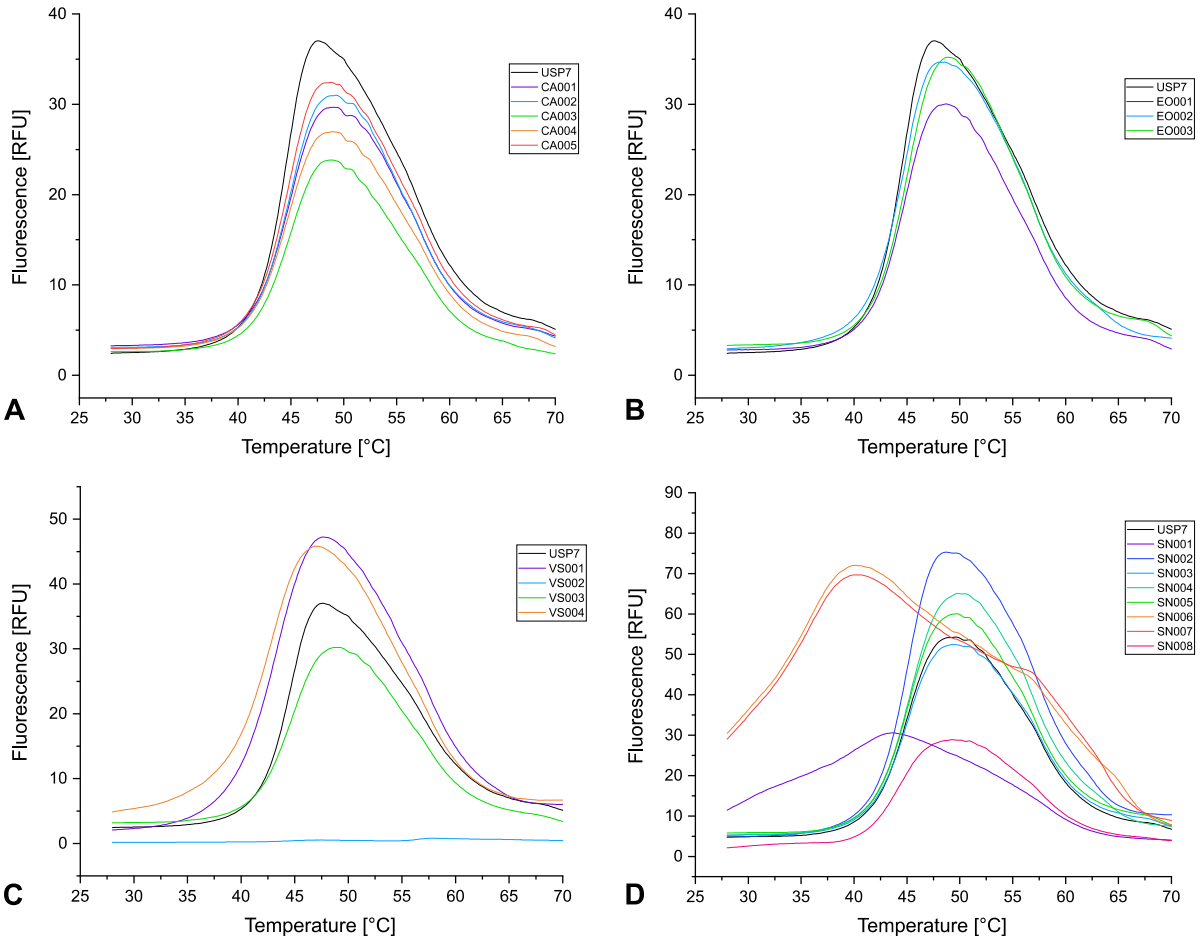

Figure S5.2: Melting curves of α-cyanoacylamides/acrylates (**A**), epoxides (**B**), vinyl sulfones (**C**), and S_NAr (**D**) fragments (1 mM) with USP7 (8 µM protein) after 30 min incubation.

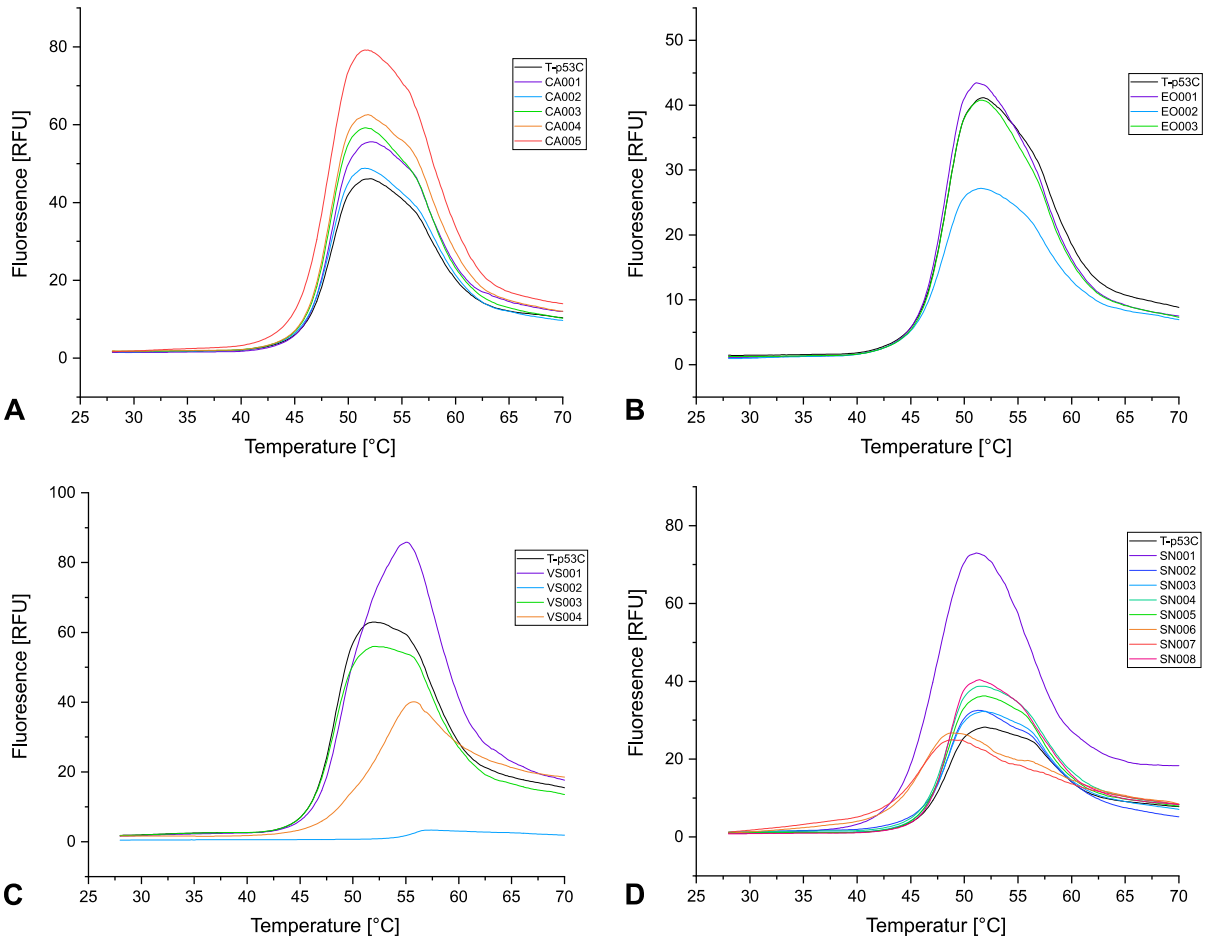

Figure S5.3: Melting curves of α-cyanoacylamides/acrylates (**A**), epoxides (**B**), vinyl sulfones (**C**), and S_NAr (**D**) fragments (1 mM) with T-p53C (8 µM protein) after 30 min incubation.

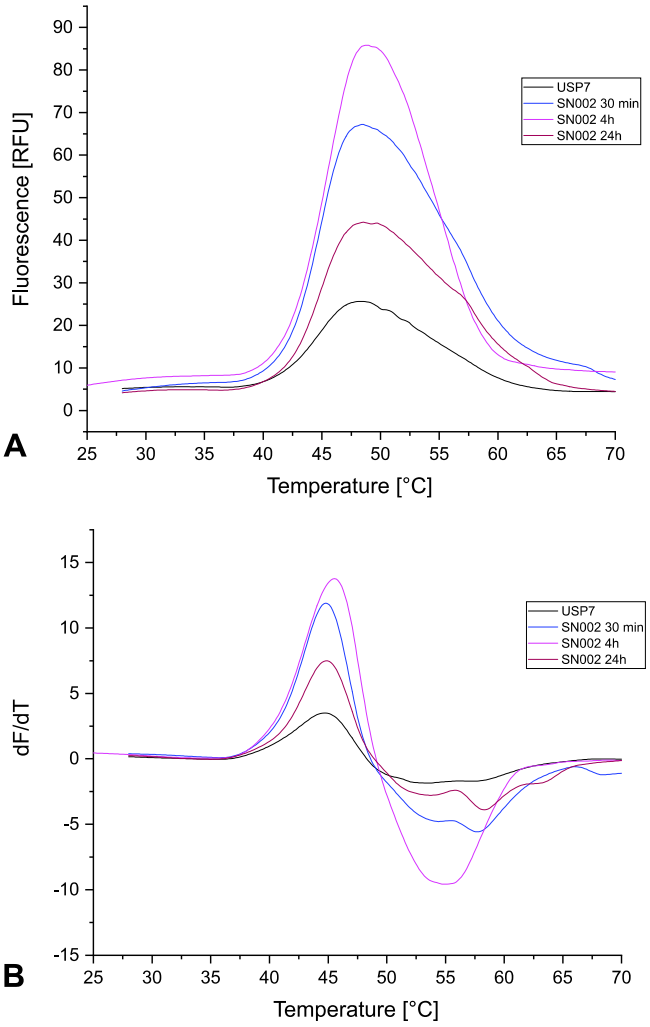

Figure S5.4: Melting curves (**A**) and first derivatives of the melting curves (**B**) of USP7 (8 µM) with 1 mM SN002 after 30 min, 4 h, and 24 h incubation at 20 °C.

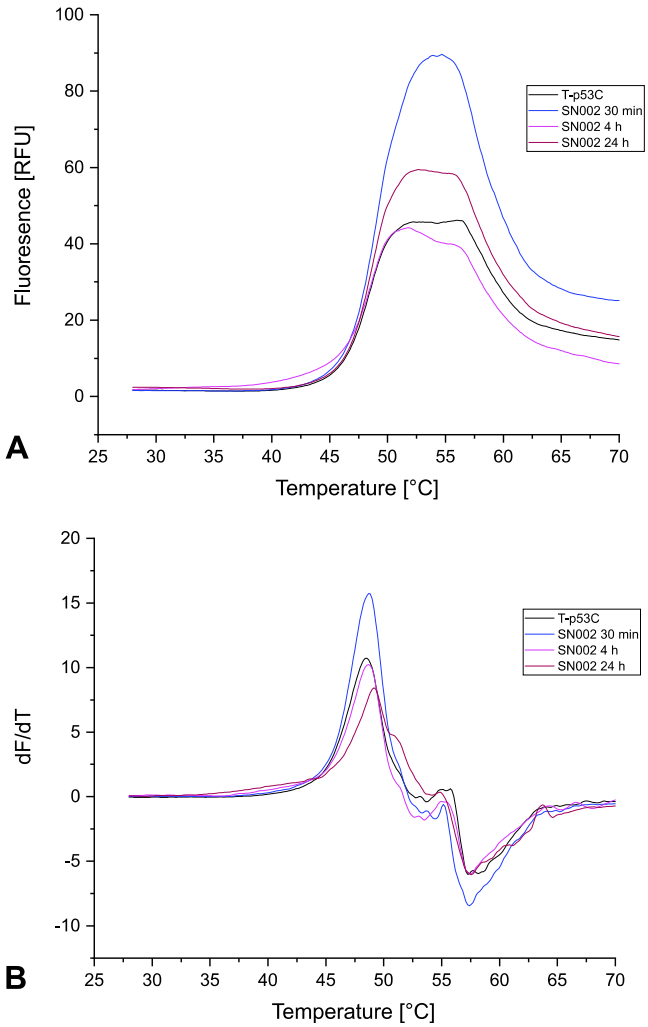

Figure S5.5: Melting curves (**A**) and first derivatives of the melting curves (**B**) of T-p53C (8 µM) with 1 mM SN002 after 30 min, 4 h, and 24 h incubation at 20 °C.

Table S5.1: ΔT_m of USP7 and T-p53C (8 µM protein) with 1 mM SN002 after 30 min, 4 h, and 24 h incubation at 20 °C

	30 min	4 h	24 h
USP7 $\Delta T_m \pm$ SD [°C]	0.22 ± 0.05	0.05 ± 0.17	0.15 ± 0.12
T-p53C $\Delta T_m \pm$ SD [°C]	0.10 ± 0.09	0.20 ± 0.09	0.40 ± 0.12

6. Intact Protein Mass Spectrometry

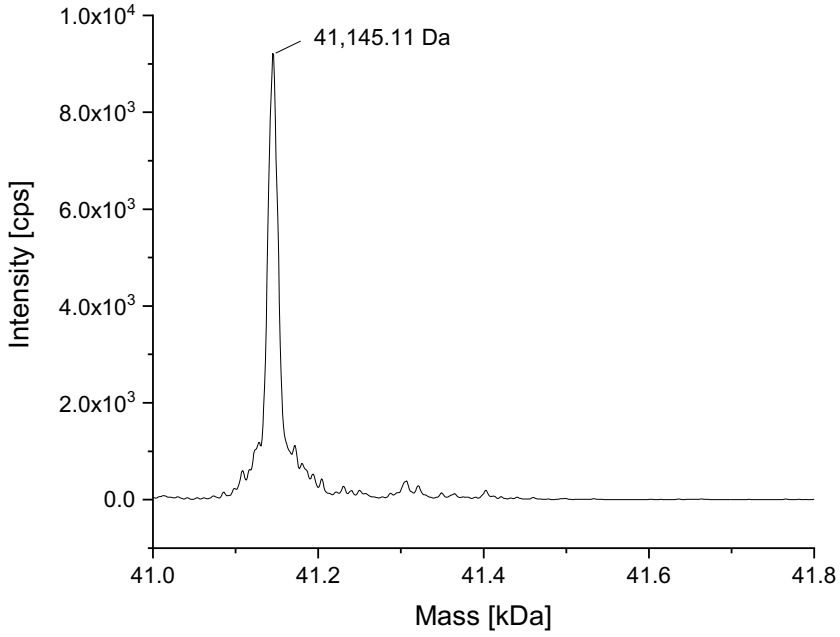

Figure S6.1: Deconvoluted MS spectrum of the intact USP7 protein. Theoretical mass: 41,145.61 Da, experimental mass: 41,145.11 Da.

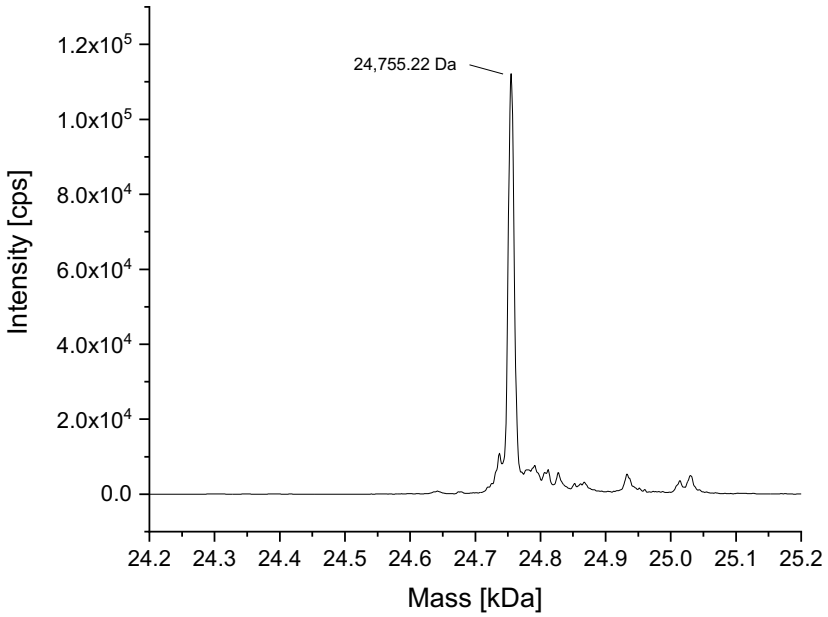

Figure S6.2: Deconvoluted MS spectrum of the intact T-p53C protein. Theoretical mass: 24,756.03 Da, experimental mass: 24,755.22 Da.